

JGR Atmospheres

RESEARCH ARTICLE

10.1029/2024JD042719

Key Points:

- The first campaign retrieval of summer water-vapor isotopes in central Greenland up to 1500 m above the ice sheet surface
- Model-observation gaps in atmospheric water-vapor isotopes can be used to identify physics understanding gaps in the Arctic
- Arctic atmospheric water vapor isotopes are informed by outside air masses, surface vapor mixing, and katabatic winds

Correspondence to:

K. S. Rozmiarek,
kevin.rozmiarek@colorado.edu








Citation:

Rozmiarek, K. S., Dietrich, L. J., Vaughn, B. H., Town, M. S., Markle, B. R., Morris, V., et al. (2025). Atmosphere to surface profiles of water-vapor isotopes and meteorological conditions over the northeast Greenland ice sheet. *Journal of Geophysical Research: Atmospheres*, 130, e2024JD042719. <https://doi.org/10.1029/2024JD042719>

Received 16 OCT 2024

Accepted 18 FEB 2025

Atmosphere to Surface Profiles of Water-Vapor Isotopes and Meteorological Conditions Over the Northeast Greenland Ice Sheet

Kevin S. Rozmiarek^{1,2} , Laura J. Dietrich^{3,4} , Bruce H. Vaughn¹ , Michael S. Town⁵ , Bradley R. Markle^{1,2} , Valerie Morris¹, Hans Christian Steen-Larsen^{3,4} , Xavier Fettweis⁶ , Chloe A. Brashear¹, Hayley Bennett¹, and Tyler R. Jones¹

¹Institute of Arctic and Alpine Research, University of Colorado Boulder, Boulder, CO, USA, ²Department of Geological Sciences, University of Colorado Boulder, Boulder, CO, USA, ³Geophysical Institute, University of Bergen, Bergen, Norway, ⁴Bjerknes Centre for Climate Research, Bergen, Norway, ⁵Earth and Space Research, Seattle, WA, USA, ⁶SPHERES Research Units, Geography Department, University of Liège, Liège, Belgium

Abstract On polar ice sheets, water vapor interacts with surface snow, and through the exchange of water molecules, imprints an isotopic climate signal into the ice sheet. This exchange is not well understood due to sparse observations in the atmosphere. There are currently no published vertical profiles of water isotopes above ice sheets that span the planetary boundary layer and portions of the free troposphere. Here, we present a novel data set of water-vapor isotopes ($\delta^{18}\text{O}$, δD , d_{xs}) and meteorological variables taken by fixed-wing uncrewed aircraft on the northeast Greenland Ice Sheet (GIS). During June–July (2022), we collected 104 profiles of water-vapor isotopes and meteorological variables up to 1,500 m above ground level. Concurrently, surface snow samples were collected at 12-hr intervals, allowing connection to surface-snow processes. We pair observations with modeling output from a regional climate model as well as an atmospheric transport and water-isotope distillation model. Climate model output of mean temperature and specific humidity agrees well with observations, with a mean difference of $+0.095^\circ\text{C}$ and -0.043 g/kg (-2.91%), respectively. We find evidence that along an air parcel pathway, the distillation model is not removing enough water prior to onsite arrival. Below the mean temperature inversion ($\sim 200\text{ m}$), water-isotope observations indicate a kinetic fractionating process, likely the result of mixing sublimated vapor from the ice sheet surface along with an unknown fraction of katabatic wind vapor. Modeled d_{xs} does not agree well with observations, a result that requires substantial future analysis of kinetic fractionation processes along the entire moisture pathway.

Plain Language Summary Water-vapor isotopes in the Arctic are powerful tools for determining the physics of the hydrological cycle. They are used to explain both climate reconstructions in ice cores and the movement of water in modern climate. Here, we provide a summer record of profiles of both water-vapor isotopes and meteorological variables above the Greenland Ice Sheet. Using models, we demonstrate that water-vapor isotopes are likely influenced not just by outside air masses but also by both upwelling sublimation and by some amount of downslope flow. An adjustment we needed to make for accurate modeling suggests that water-vapor isotope observations in the atmosphere can inform how we parameterize precipitation in water-isotope models. This work suggests the value added from atmospheric water isotope observations to understanding not just water source-and-sink but also water source-to-sink in the Arctic.

1. Introduction

The hydrological cycle is changing quickly in response to anthropogenic climate drivers and the associated Arctic amplification (Allan et al., 2020; Vihma et al., 2016). An important state variable of the hydrological cycle is the water isotopic composition. As water is continually redistributed through the hydrologic cycle, its isotopic composition is altered due to phase changes and mixing, providing a forensic lens from which to extract climatic information (Jouzel et al., 2013; Galewsky et al., 2016; S. Dee et al., 2023). Water stable isotopes preserve integrated memory of the undergone hydrological processes; thus, they reconcile physics and thermodynamics not explained by traditional meteorological variables (temperature, humidity, pressure, and wind). Ill-constrained physics implemented in isotope-enabled models will be reflected in their isotope simulations and, vice versa, the correct implementation of model physics is thus vital for using water isotope-enabled models to make statements about the climate's past and future. Although a Global Network of Isotopes in Precipitation (GNIP) has

been developed, which has been used extensively to test model skill, very few records of water-vapor isotopes are available (Bowen et al., 2019). One reason for the lack of vapor-isotope records is that the retrieval of vertically resolved isotope profiles in the atmosphere is a logistical and technical challenge. Harder yet are vertical profiles in the Arctic, where the hydrological cycle intersects with one of its largest reservoirs, the Greenlandic Ice Sheet (GrIS). To date, there are no vertically resolved data sets of water-vapor isotopes in the Arctic besides scattered observations (Rozmiarek et al., 2021).

Most in situ water-vapor isotope studies have occurred at lower latitudes, partly due to the ability to fly instrumented, crewed aircraft at low altitudes. Such vapor-isotope measurements have allowed for disentangling the causes of regional-precipitation changes, which occur either from thermodynamic (phase-change fractionation due to a change in temperature) or dynamic (i.e., advection and mixing) processes (S. G. Dee et al., 2018; Risi et al., 2020). However, many knowledge gaps still exist that vapor isotopes can inform, such as vertical mixing (Galewsky & Hurley, 2010; Risi et al., 2013), deep convective detrainment (Bony et al., 2008; Hu et al., 2022; Schmidt et al., 2005), precipitation re-evaporation (J. Worden et al., 2007; Field, 2010), and satellite retrieval algorithms (J. R. Worden et al., 2019). To push the utility of vapor isotopes forward, continuous measurements from towers (anywhere from 2 to 25 m height) have occurred, such as a multi-year network (since decommissioned) that operated in Bermuda, Iceland, and in the Arctic in Greenland and Svalbard (Leroy-Dos Santos et al., 2020; Steen-Larsen et al., 2013, 2015). Tower-based Arctic vapor isotope measurements have been correlated to sea ice extent and synoptic moisture transport (Akers et al., 2020; Klein et al., 2015). Atmosphere water-vapor isotope profiles exist, but at lower latitudes, meaning they have limited use in representing higher Arctic latitudes (Henze et al., 2022; Salmon et al., 2019; Sodemann et al., 2017). The success of using water-vapor isotopes in lower latitudes and in a limited capacity in the Arctic justifies a community need for more Arctic water-vapor measurements. One such location is over the accumulation zone of the GrIS, as there are mechanisms unique to ice sheets that may differ from model-physics derived from studies done elsewhere.

With a warming climate, the GrIS will play an important role in Arctic hydrology, and consequently, Greenland has become a focus of recent water-isotope research as a constraint on energy and mass balance. Vapor exchange with the near surface atmosphere has been shown to leave behind an imprint in the isotopic composition of Greenland surface snow (Hughes et al., 2021; Steen-Larsen et al., 2013, 2014; Wahl et al., 2021). This imprint is significant enough that it may impact the appearance of climate signals as a post-depositional effect in ice cores (Dietrich et al., 2023; Town et al., 2008, 2024; Wahl et al., 2022). How much exchanged vapor leaves the ice sheet? Estimations vary, particularly when considering a warming climate (Boisvert et al., 2017; Zolles & Born, 2022). Kopec et al. (2022) show convincing evidence from snow pits and snow cores that the sublimated snow from upwind on the Greenland ice sheet influences the isotopic content of snow at Summit, Greenland. However, a direct link between atmospheric vapor and the snow surface is not made. A recent study in the accumulation zone of the GrIS at the EGRIP ice core camp found that as much as 31% of snow deposition was sublimated during the summer (Dietrich et al., 2024). Where does this vapor go? To answer that question, we need to obtain observations of water-vapor isotopes profiles above the GrIS, extending above altitudes much higher than typical tower setups. Because of safety and logistical constraints associated with the GrIS, such measurements can only reliably and routinely be made with uncrewed aerial systems (UAS) or “drones” (Rozmiarek et al., 2021).

Toward evaluating the modeling utility of water-vapor isotopic profiles over the GrIS, our research team utilized a fixed-wing drone to measure 104 vertical profiles of meteorological data (temperature and humidity) and water-vapor isotopes to altitudes as high as 1,500 m during summer 2022 at the EGRIP ice core camp in interior northeast Greenland. We also measured snow-water isotopes at 12-hr intervals at 1 and 5 cm depths. We use the observations as constraints on a Lagrangian back trajectory model coupled to a water distillation model, HySPIT-SWIM (Markle & Steig, 2022). By using water-vapor isotope observations to apply a correction to the amount of precipitation experienced by a moisture parcel along its trajectory, we demonstrate the value of water-vapor isotopes to informing hydrological system models. Additionally, we present evidence of the imprint of surface sublimation into the water-vapor isotopic composition of the atmospheric column. To evaluate meteorological profiles, we compare observations to a polar regional climate model, the Modèle Atmosphérique Régional (MAR) at the native resolution of 13 vertical levels up to 1,500 m, and novelly at 28 levels. Across all isotope and meteorological model-observation pairings, we demonstrate the use of water-vapor isotope profiles in identifying model physics gaps in Greenland.

2. Methods

2.1. Site Description

Measurements were conducted from June 6 to 10 July 2022 at the East Greenland Ice Core Project (EGRIP) drilling site (75.63°N, 36.00°W; altitude ~2,700 m a.s.l.) at the onset of the North-East Greenland Ice Stream (NEGIS) in an accumulation zone. At the EGRIP site, an automated weather station recorded near-surface meteorological conditions as part of the Program for Monitoring of the Greenland Ice Sheet (PROMICE, Fausto et al. (2021)). During the study period, the average 2 m temperature was -12.5°C with diurnal means between -21.0 and -3.8°C . The average 2 m relative humidity was 75.9% with diurnal means between 67.0% and 86.6%. Estimates of the annual accumulation rate at EGRIP range from 134 to 157 mm/year of liquid water equivalent (l.w.e.) (Komuro et al., 2021), 138 mm/year l.w.e (Nakazawa et al., 2021), and 135 mm/year l.w.e (Town et al., 2024).

2.2. Water Isotopes

Water-isotope measurements are expressed as the ratio of rarer, heavier, isotopes relative to their lighter and more common counterparts, for example, $^{18}\text{O}/^{16}\text{O}$ or $^2\text{H}/^1\text{H}$ (commonly D/H where D is deuterium). These ratios are commonly reported in δ notation (Equation 1, Craig (1961)) which expresses their value relative to internationally recognized primary reference materials, Vienna Standard Mean Ocean Water (VSMOW) normalized to Standard Light Antarctic Precipitation (SLAP), as outlined by the IAEA. To tie measurements to primary reference materials, a suite of secondary reference waters is maintained and rigorously calibrated to VSMOW2 and SLAP2. Secondary reference waters are stored in accordance with guidelines described in IAEA technical note no. 43 (Newman et al., 2009)).

$$\delta_{\text{sample}} = \left[\frac{R_{\text{sample}}}{R_{\text{VSMOW}}} - 1 \right] \quad (1)$$

In δ notation, δD and $\delta^{18}\text{O}$ refer to deviations from primary reference materials (standards) expressed in parts per thousand (per mille or ‰). The second order isotope parameter d (deuterium excess, d-excess) is calculated as $d = \delta\text{D} - 8 * \delta^{18}\text{O}$ (Dansgaard, 1964).

2.3. Airborne Water-Vapor Sampling and Radiosonde

Aerial water-vapor sampling was conducted following the methodology of Rozmiarek et al. (2021). A fixed-wing uncrewed aerial system (UAS, or drone), manufactured by Black Swift Technologies (model S2), was used to fly a custom air-capture payload with four glass sampling flasks to altitudes of 1,500 m above ground level (AGL) over the EGRIP site. The system was modified from Rozmiarek et al. (2021) to include a Vaisala RSS-421 radiosonde which measured temperature and relative humidity with improved accuracy and precision over on-board aircraft instruments. The UAS relays live data to inform flight operators about the structure of the atmosphere. Operators then generally choose to capture air in the center of atmospheric layers whose boundaries are identified by distinct changes in the boundary layer (e.g., potential temperature, humidity). As the aircraft is susceptible to riming, the flight ceiling was often limited by cloud heights, determined by sight and an intermittently available (due to technical difficulties) Vaisala CL-31 ceilometer at the EGRIP camp. The riming limitation of the drone platform is an operational filter on the conditions sampled. During each flight mission, in addition to the four flask samples taken by the drone, three to four additional flask samples were taken near the ground level at 2 m AGL.

Each flask sample of atmospheric air is 550 cubic centimeters. Before sample collection, each flask is flushed with sample air for 10 flask volumes over 1.5 min to minimize memory effects. For airborne sampling, the UAS orbits (60 m radius) at constant altitudes during flushing and sample acquisition. After flight, the samples are analyzed on a Picarro L2130-i cavity ring-down spectroscopy (CRDS) instrument for 12 min at a ~30 sccm flow rate. The first and last 3 min of the analysis are removed to prevent memory and mixing effects, and the remaining 6 min are averaged to get isotope and humidity measurements. Several liquid water-isotope standards were available to calibrate measurements to the VSMOW-SLAP scale. A flash evaporator diluted with dry air was used to generate water-vapor at different specific humidities (1,000–40,000 ppm) from the liquid water-isotope standards. For additional details, see Appendix A and Rozmiarek et al. (2021).

To address the potential for spatial nonconformity, experiments were performed at similar altitude (200 m) at various distances up to 2 km away from the standard take-off location. Isotope results from experiments were within the first standard deviation for the isotope sampling system ($\delta^{18}\text{O}$ 0.45‰ and δD : 2.8‰, Rozmiarek et al. (2021)), indicating that spatial homogeneity was given within a few kilometers of the EGRIP sample site during the duration of any flight during the June–July sampling period.

2.4. Surface Snow Sampling

Surface snow samples were taken in the morning and evening during the study period. Samples were taken at two depths, 1 and 5 cm, at 11 different locations 5 m apart from each other in a protected “clean snow” region of camp. These samples are unlikely to be correlated spatially due to the typical size of surface features at EastGRIP (Zuhr et al., 2021, 2023). Snow samples were melted and transferred to 2 mL vials. Liquid samples were then shipped and measured at the Stable Isotope Lab at the University of Colorado Boulder. Samples were analyzed on a Picarro L2130-i CRDS coupled to an HTC PAL auto sampler injection system (CTC Analytics) and Picarro V1102-I vaporization module. Each sample was measured with the calibration scheme outlined in Rozmiarek et al. (2021). Individual vials were subsampled for six total injections, where the last three injections are averaged to avoid memory effects (Schauer et al., 2016). Measurements averaged for the last three samples have uncertainties of 0.1‰ $\delta^{18}\text{O}$ and 1‰ δD .

2.5. Cloud Mask

Cloud occurrence is used to bin atmospheric measurements into clear and cloudy periods, with a reminder that the UAS platform was only flown in favorable conditions. As such, the cloud mask is not separating all clear-sky conditions from all cloudy conditions, but rather separating all clear-sky conditions from some mildly cloudy conditions. The cloud mask used for this binning was determined using hourly longwave downwelling irradiance fluxes (LDF) from a PROMICE automated weather station at the EGRIP site (Fausto et al., 2021). The cloud mask is based on the ground-based analysis method for cloud detection from LDF measurements from Town et al. (2007). Thresholds for 6-hourly mean LDF (LDF_μ) and 6-hourly standard deviation LDF_σ are used together to filter clear sky periods from all other periods. The governing principle behind this cloud mask is that the LDF responds sensitively to the presence of clouds; clear sky periods experience low LDF_μ and small LDF_σ . Periods fully overcast with optically thick clouds experience high LDF_μ and small LDF_σ . All other periods experience a range of mean 6-hourly mean LDF but have higher variability than a clear sky period. The LDF_μ is sensitive to both the clear-sky temperature and humidity profiles. Therefore, we include monthly mean LDF_μ thresholds to accommodate changes in atmospheric composition and structure (Town et al., 2007); $LDF_{clear,Jun} = 215\text{W/m}^2$, $LDF_{clear,Jul} = 225\text{W/m}^2$. The impact of cloud variability on LDF does not vary significantly from month to month, so we use the same 6-hourly LDF_σ threshold for both June and July (7W/m^2). The variability threshold is particularly important for filtering out periods of low 6-hourly mean LDF_σ (e.g., optically thin scattered clouds). These clouds may not have an appreciable impact in surface temperature, but they likely have an impact on the isotopic content of the boundary layer (Quadrant II in Figure B3).

2.6. MAR Model

We evaluate the accuracy of temperature and humidity in the regional climate model MAR (version 3.12) by comparing to UAS observations (Modèle Atmosphérique Régional, e.g., Fettweis et al. (2017)). MAR was specifically designed for regional simulations in polar regions and is a well-established tool to simulate the GrIS climate and surface mass balance (Fettweis et al., 2013). Snow-atmosphere interactions of energy and mass are simulated by the atmosphere-surface transfer scheme SISVAT (Soil Ice Snow Vegetation Atmosphere Transfer, Gallée and Schayes (1994); Fettweis et al. (2005)) that is coupled to the atmospheric module of MAR. MAR is forced in the atmosphere at its lateral boundaries by reanalysis product ERA-5 at 6-hr intervals. The simulated area for this study covers the whole GrIS at a horizontal resolution of 15 km. The simulation is initialized and driven at its boundaries with the reanalysis product ERA-5 (Hersbach et al., 2020). We use two different simulation setups to evaluate the performance of simulations with different vertical resolutions. In the first simulation, MAR runs on a standard vertical resolution of 24 vertical levels, of which 13 are below 1,500 m, down to 2 m. In the second simulation (denoted MAR_hr), MAR runs on a vertical resolution of 40 levels, of which 28

are below 1,500 m down to 2 m. The spacing between the vertical levels is fine close to the surface and increases with height (e.g., 1.9 m, 5.7 m, 9.6 m, 18.0 m, 33.6 m, ..., 922.0 m, 1,439.2 m, and 2,134.6 m).

2.7. HySPLIT-SWIM

To produce realizations of the water-vapor isotopic composition of the atmosphere 1,500 m above EGRIP, we combine Lagrangian back-trajectories of air masses with a water-isotope distillation model. We present 10-day back-trajectories at eight different heights above the ice sheet (10, 50, 100, 200, 500, 1,000, 1,500, and 2,000 m above the ice surface) using the NOAA HySPLIT model (Draxler & Hess, 1998), at 6 hourly intervals for all days spanning the observational period. Meteorological variables for each trajectory were determined by HySPLIT from the underlying reanalysis (NCEP/NCAR) and then used to force the Simple Water Isotope Model (SWIM; Markle & Steig, 2022). Based on these inputs, SWIM simulates pseudo-adiabatic pathways, allowing for water removal through condensation that a moist air parcel undergoes as it travels in thermodynamical space. We select HySPLIT-SWIM as it incorporates the best-to-date assumptions of water-isotope distillation along a moisture parcel's trajectory, which are the same assumptions used in ice core temperature reconstructions (Markle & Steig, 2022). HySPLIT-SWIM has previously been tested against precipitation observations but has not been tested against water-vapor isotopes, which we do for the first time in this study. SWIM does not consider mixing between the air parcels or interaction of the modeled vapor with the surface. Thus, these modeled results, in comparison to observations, may serve as a reference point to consider the effect those processes may have on the near-surface troposphere water-vapor isotopic composition.

The pseudo-adiabatic cooling pathways used by SWIM are defined by initial and final temperatures. Although the 10-day back-trajectories are longer than the median residence time of water in the atmosphere globally, we cannot represent the full distribution of lifetimes of all water molecules in the parcel. Back trajectory results thus guide the assumptions used to initialize SWIM water isotopic values. To test the effect of initialization assumptions, we examine two different simplistic though reasonable vapor initialization choices: (a) we initialize water vapor within the distillation model at the air temperature of the last point when the trajectory was within the boundary layer over the ocean, (b) we initialize water vapor at the warmest point of the trajectory that is also within the boundary layer over the ocean (and thus likely with highest specific humidity). Other source conditions and along-path parameters such as ice/liquid fraction of condensate and supersaturation conditions are calculated using the base assumptions of the SWIM as outlined in Markle and Steig (2022).

Moisture is removed from the distillation model, and water isotopes fractionate, whenever the air parcel cools enough to reach saturation or a prescribed level of supersaturation. The model is then run forward for each temperature pathway defined by each back-trajectory and the final vapor conditions of the column above the ice sheet. Similar to our testing of assumptions about the initial conditions, we test three possible choices for the lowest temperature bound along the distillation path. In the first, v1, we use the naïve assumption of the final temperature suggested by the back-trajectory. Since the air parcel may reach a colder temperature and condense more vapor along the trajectory before reaching the observation site, in the second test, v2, we use the coldest temperature along the back-trajectory to set the total amount of moisture removal.

Finally, we recognize that although idealized pseudo-adiabatic cooling represents air at saturation, the real atmospheric column above the ice sheet is on average sub-saturated with respect to water. Thus, the model retains more moisture in the atmosphere than the observations and so more moisture must be removed along the distillation path than suggested by pseudo-adiabatic cooling alone if the moisture content of the modeled and observed atmosphere are to be compared directly. In a third test, v3, we apply a small adiabatic adjustment to cool the air parcel and condense enough moisture such that the final moisture content is consistent with the sub-saturated average of our observations. As a reference, the average relative humidity of the observations in the 1,500 m column is 68.7%. Each arriving air parcel to EGRIP is cooled, causing moisture to be removed such that the final relative humidity, if the parcel is warmed in isolation back to the arrival temperature, matches the binned average relative humidity of observations at that altitude. It is worth noting that using a fixed sub-saturated final relative humidity at all altitudes (e.g., 65%, the 1,500 m column observation mean), yields qualitatively similar results. Conceptually this thermodynamic adjustment may be consistent with air subsidence (and thus re-warming to the final temperature) over the site. These three tests are not equally likely, the third is the most physically justifiable and most constrained by empirical data. However, the range of results shown later from these tests

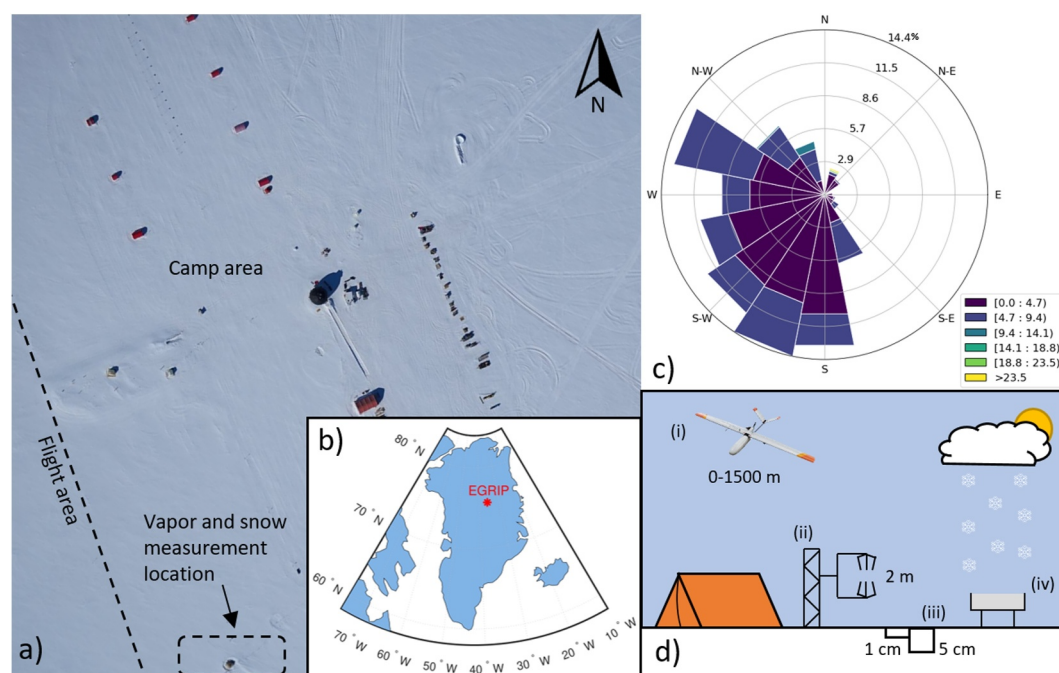


Figure 1. (a) Aerial overview of the EGRIP camp area. The area in which UAS data (“Flight area”), vapor measurements, and snow samples were obtained are outlined. (b) Location of the EGRIP camp on the GrIS. (c) Wind distribution and velocities (m/s) at EGRIP during the observational period. (d) Schematic overview of the different surface and atmospheric measurements that were taken during the campaign. (i) UAS flask sampling of water vapor isotopes between 0 and 1,500 m above ground level (AGL). (ii) Met station. (iii) Snow sampling at 12 hr intervals at 1 and 5 cm depths. (iv) Precipitation capture for snow isotopic sampling.

demonstrate the range of impact that assumptions about the total cooling and moisture removal pathway has on the interpretation of results.

2.8. Binning Data by Distinct Weather Events

To assess how sensitive the shape of the average summer profile (i.e., the average of all data collected in the study period) is to individual weather events, we bin data into different meteorological periods. Periods are defined by one or more of the following: meteorological variables (air temperature, air relative humidity, and precipitation), isotope values ($\delta^{18}\text{O}$, δD), if weather was appropriate for flight missions, precipitation events, and finally by MAR-determined changes in specific humidity above the near-surface planetary boundary layer. Partitioning in this way is intended to separate distinct air masses, which may contain separate isotopic relationships with altitude. Regions and justifications are listed in Table B1 and shown in Figure B4.

3. Results

3.1. Meteorological and Water-Isotope Profiles

Although there are day-to-day variations, there exists a common average atmospheric structure above EGRIP camp during the observational period, from June 6 to 10 July 2022, viewed through the lens of an operational filter of “clear sky” or “high clouds” conditions enabling flight missions. The height-binned average of temperature and humidity measurements from 104 flights are shown in Figure 2. The polar atmosphere above EGRIP is generally stable with the most stable conditions in the lower 200 m, evidenced by potential temperature (Figure 2b). An atmospheric temperature inversion layer exists immediately above the near-surface layer of a few meters in height to ~ 200 m. The existence of an inversion layer is consistent with previous expectations for an interior ice sheet site, where a cold surface cools a warmer near-surface atmosphere (Moore et al., 2013). Within the inversion layer (~ 2 to ~ 200 m), the temperature increases at a rate of 0.39 K/100m. Above ~ 200 m, the stability weakens, and the temperature decreases at a rate of -0.46 K/100m.

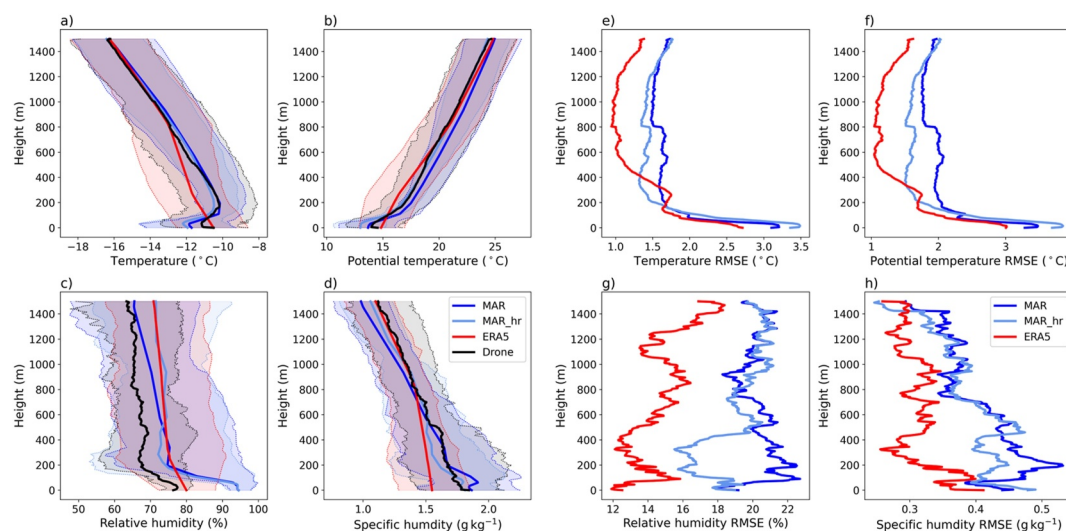


Figure 2. Left: Vertical profiles of (a) temperature, (b) potential temperature, (c) relative humidity, and (d) specific humidity averaged over 104 flights as measured by the aircraft (black) and simulated by MAR (blue), MAR_hr (light blue), and ERA-5 (red). Shading indicates interdecile range of variability across the different flights. Right: Vertical profiles of the RMSE between modeled and observed (e) temperature, (f) potential temperature, (g) relative humidity, and (h) specific humidity across 104 flights for MAR (blue), MAR_hr (light blue), and ERA-5 (red).

We observed a large range of atmospheric isotopic values during the observational period, with values varying between -398.95 and -251.17‰ for δD , -54.19 and -30.37‰ for $\delta^{18}\text{O}$, and -9.81 and 63.65‰ for d_{xs} . Figure 3 shows summer 2022 isotopic profiles at EGRIP separated to include (1) clear-sky days and (2) cloudy days when flight operations were still possible below the bottommost cloud layer. Averaging the values of $\delta^{18}\text{O}$ and δD into 50 m bins during flights determined to have a cloud layer reveals an “inverse C-shape” pattern that is not apparent during clear-sky periods. The $\delta^{18}\text{O}$ and δD for flights with a cloud-layer above exhibit an increase with height up to ~ 200 m, a layer with variable values from 200 to 850 m, and a decrease with height above 850 m; this forms the “inverse C-shape”. Conversely, the binned d_{xs} is high close to the surface, decreases with height up to approximately 200 m, is nearly constant between 200 and 850 m, and increases above 850 m, forming

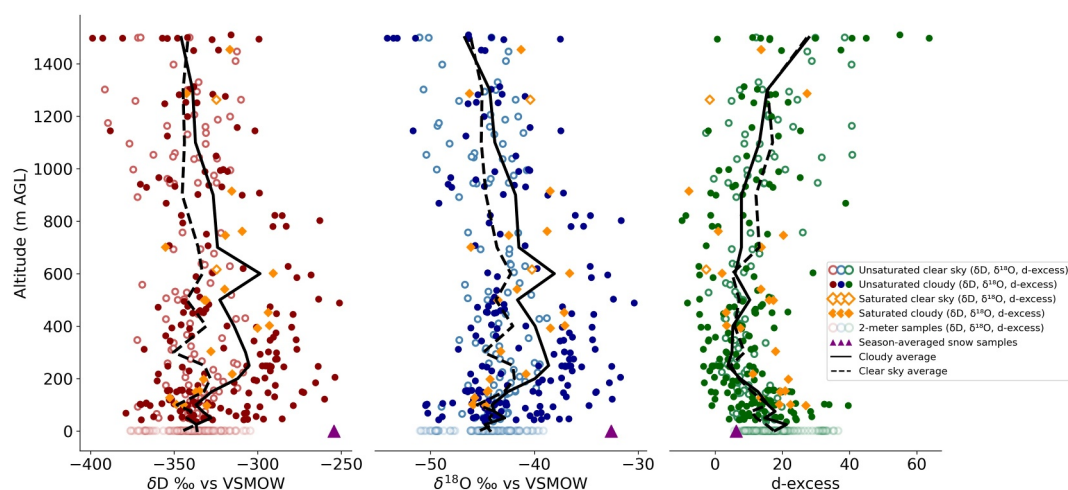


Figure 3. All isotopic UAS samples for δD (left), $\delta^{18}\text{O}$ (center), and d_{xs} (right). Orange diamonds indicate isotopic samples that were taken in saturated conditions with respect to ice ($RH_{\text{ice}} = 100\%$). Open dots and diamonds indicate clear sky conditions. Closed dots and diamonds indicate cloudy conditions. Lines denote two trend lines: (1) dashed for clear sky conditions and (2) solid for cloudy conditions. Average 5 cm snow values are shown as a purple triangle. 2 m vapor samples taken during flight mission at the 2 m surface level are plotted as open circles with a small opacity to indicate density of observations.

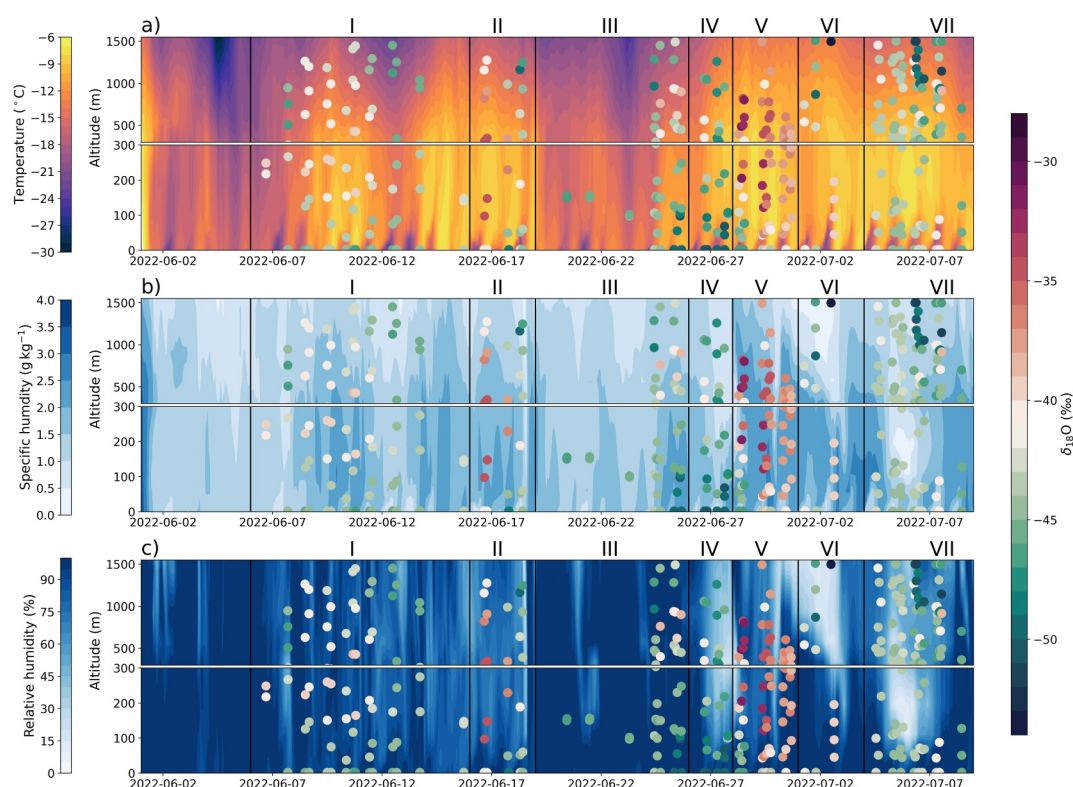


Figure 4. MAR_hr model runs at hourly resolution compared to observations of water vapor dxs during the duration of the sampling period. (a) Atmospheric temperature ($^{\circ}\text{C}$), (b) atmospheric specific humidity ($\frac{\text{g}}{\text{kg}}$), and (c) atmospheric relative humidity (%). Dots: Isotopic measurements of $dxs(\text{‰})$. Measurement periods are defined in numeral above.

an “forward C-shape”. The dxs “forward C-shape” is evident in many individual profiles over the observational period, though its relationship to meteorological variables is less clear (Figure 4).

To determine if correlations exist between isotopes and meteorological variables, we compare the measured values of $\delta^{18}\text{O}$ to temperature and humidity (Figures 5a and 5b). The values of $\delta^{18}\text{O}$ correlate slightly with the specific humidity ($R = 0.6$, $p < 0.001$), Figure 5a). This correlation is significantly higher than the weak correlation between the temperature and $\delta^{18}\text{O}$ ($R = 0.39$, $p < 0.001$). We also compare $\delta^{18}\text{O}$ to dxs to determine to what extent kinetic fractionation relates to total fractionation which is represented coarsely by lower $\delta^{18}\text{O}$ values for more fractionation. The resulting linear relationship between dxs and $\delta^{18}\text{O}$ correlates well ($R = 0.75$, $p < 0.001$) and is consistent with the concept of a local meteoric water line (Putman et al., 2019). We observe an increasing spread of dxs values toward lower values of $\delta^{18}\text{O}$. This indicates that air parcels which have experienced the most distillation have also experienced the most variability in kinetic isotope effects.

3.2. Water Isotopes of Surface Snow

Surface snow was measured at 1 and 5 cm depths at 12-hr intervals to provide context relative to UAS water-vapor isotope measurements (Figure 6). Throughout the observational period, the measured values of $\delta^{18}\text{O}$ in the surface snow varied but in generally increased with an average rate of 0.19 ‰/day between June 6th (−33.8‰) and July 8th (−30.61 ‰) in the top 1 cm, and in the top 5 cm with an average rate of 0.16‰/day between June 6th (−36.3‰) and July 8th (−31.13‰) (Figure 6b). The observed values of $\delta^{18}\text{O}$ in the top 1 cm and fresh precipitation are consistently more positive than in the top 5 cm, except for a period in the end of June (6/25–6/28) with relatively high amounts of fresh snowfall (6/17–6/28). Because of the low density of fresh snow, the consistent difference between surface and sub-surface snow during periods with less precipitation is likely due to the combination of the delay time that the isotope signal has to propagate by diffusion from the surface to 5 cm snow depth. For context, the accumulation at EGRIP is 45.6 ± 3.8 cm, but weighted toward summer and autumn

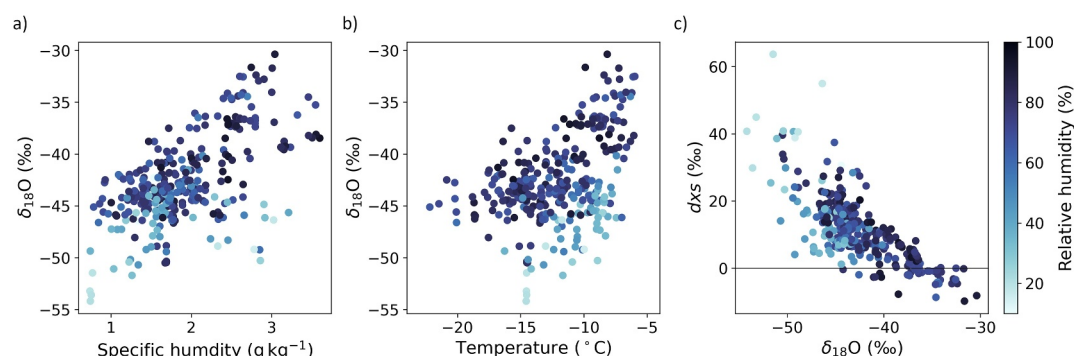


Figure 5. Isotopic composition from UAS air samples, as well as atmospheric specific humidity, and temperature measurements taken contemporaneously with the radiosonde integrated into the UAS. (a) Atmospheric specific humidity (g kg^{-1}) scattered against $\delta^{18}\text{O}$. (b) Atmospheric temperature ($^{\circ}\text{C}$) scattered against $\delta^{18}\text{O}$. (c) $\delta^{18}\text{O}$ scattered against dxs . In all three plots, colors show the atmospheric relative humidity with respect to water.

(Town et al., 2024). During the entire observational period, the observed $\delta^{18}\text{O}$ values in the snow samples varied between -34.3 and -27.2 ‰ in the top 1 cm, and between -37.0 and -31.0 ‰ in the top 5 cm.

The dxs of surface snow tracks its source history, fractionation history of a precipitating air-parcel, and the post-depositional fractionation history of the snow itself (Hu et al., 2022; Merlivat & Jouzel, 1979; Town et al., 2024).

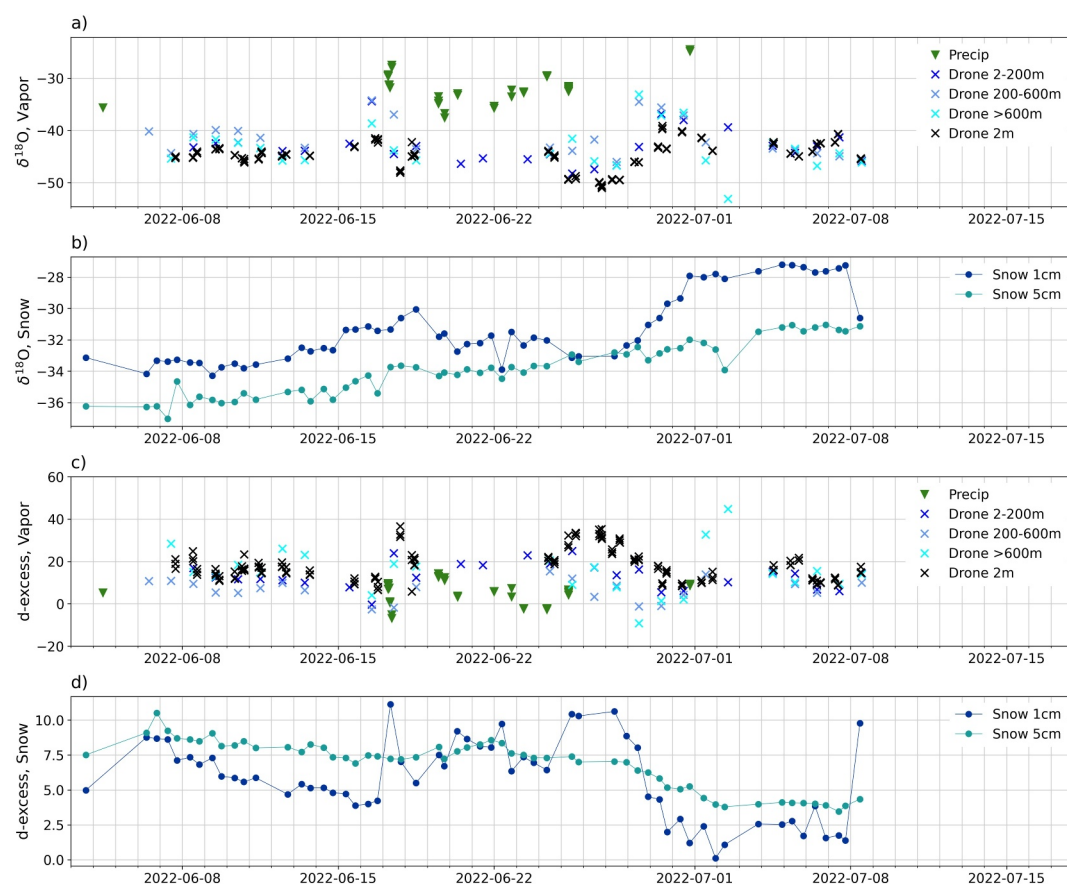


Figure 6. Overview of all isotopic measurements of the atmospheric vapor $\delta^{18}\text{O}$ (a) and dxs (c), and the snow $\delta^{18}\text{O}$ (b) and dxs (d) in the observational period. Green triangles show collected precipitation samples. Black crosses show the ground flask samples taken contemporaneously with the UAS air-capture flights. The UAS air samples are shown for three different height layers between 2 and 200 m in dark blue, between 200 and 600 m in light blue, and above 600 m in light turquoise.

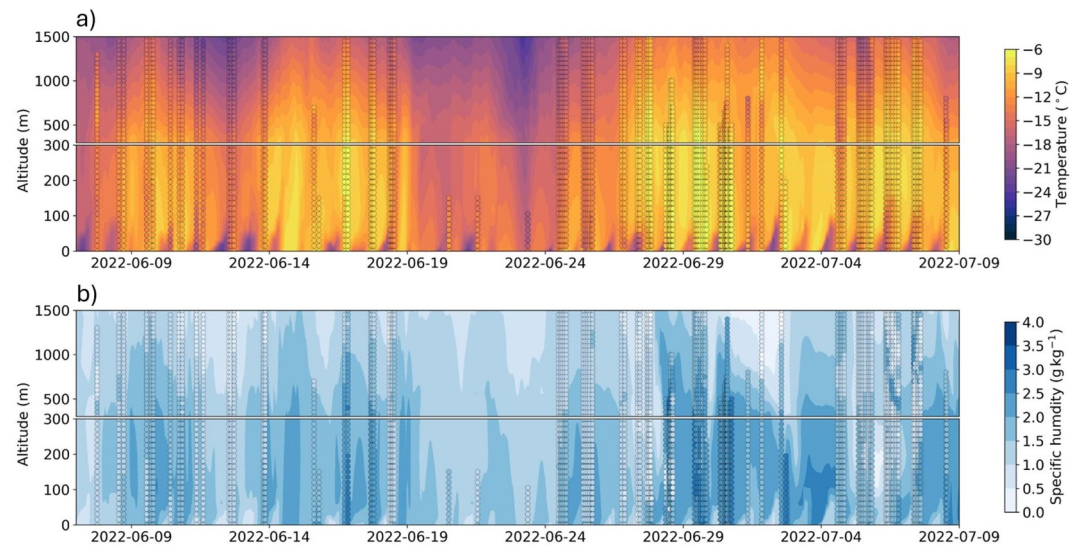


Figure 7. (a) Temperature ($^{\circ}\text{C}$) and (b) specific humidity ($\frac{\text{g}}{\text{kg}}$) simulated with the MAR model in the observational period. The dots show height binned UAS data with a bin size of 15 m below 300 m height, and 50 m bins above 300 m height.

The dxs signal decreases over the observational period with an average rate of $-0.12\text{‰}/\text{day}$ between June 6th (8.73‰) and July 8th (9.79‰) in the top 1 cm and with an average rate of $-0.17\text{‰}/\text{day}$ between June 6th (9.8‰) and July 8th (4.34‰) in the top 5 cm (Figure 6d). However, the decrease is not consistent over the period and dxs in the top 1 cm (1σ standard deviation of 2.79‰) is more variable than in the top 5 cm (1σ of 1.75‰), with a continuous decrease between 6/6–6/16, no significant trend between 6/17–6/27, and a notable decrease between 6/28–7/1, plateauing afterward until 7/7. During the entire observational period, the observed dxs values in the snow samples varied between 0.1 and 11.1‰ in the top 1 cm, and between 3.5 and 10.5‰ in the top 5 cm. This result matches Town et al. (2024), where snow dxs was found to decrease in value throughout the summer post-deposition. When compared to observations of vapor isotopes, both near-surface (0 to ~ 2 m) and up to 1,500 m observations were near consistently higher dxs relative to surface snow measurements and consistently lower $\delta^{18}\text{O}$ and δD .

3.3. Comparison of EGRIP Sonde Data to MAR and ERA-5

We contrast the average temperature and humidity of all flights over the entire sampling period against the regional polar-climate model MAR and the climate reanalysis product ERA-5 (Figure 7). We examine the statistical ability of both products to represent the average meteorological structure of the atmosphere up to 1,500 m above EGRIP. Comparisons are made for heights at which observations are available. On average, both MAR and ERA-5 compare well with 5 m binned UAS observations at higher altitudes but worse closer to the surface. MAR has a lower average temperature and specific humidity bias (difference of $+0.10^{\circ}\text{C}$ and -0.043 g/kg , or -2.91%) than ERA-5 -0.42°C and -0.121 g/kg , -8.23%), especially at lower altitudes from 0 to 600 m above the surface. Below 600 m, ERA-5 has a larger temperature negative bias -0.63°C and specific humidity negative bias (-0.15 g/kg , -9.05%) compared to observations, whereas MAR captures the average temperature and humidity in this level well, $+0.15^{\circ}\text{C}$ and $+0.03\text{ g/kg}$ ($+2.05\%$). The likely reason for this difference between the models is that MAR has a higher vertical resolution close to the surface (11 atmospheric levels in the lower 600 m, 25 levels for MAR_hr) compared to ERA-5 (2 levels in the lower 600 m), and thus captures the surface boundary layer vertical variability better. However, MAR has a positive bias in the relative humidity with respect to water of $+5.7\%$ averaged over the whole profile which is stronger for observations in the lower 200 m ($+13.0\%$).

Locating the height of the typical mean temperature inversion is of critical importance, as moisture transport across that boundary to the atmospheric layer above is attenuated. Binned 5 m UAS profiles indicate that the temperature inversion occurs at ~ 200 m. MAR captures this temperature inversion, whereas ERA-5 cannot resolve the average inversion due to its low vertical resolution. Further, the UAS data indicates the highest temperature variability over the sampling period close to the surface ($\sigma_{\text{max}} = 9.7^{\circ}\text{C}$ at 15 m), decreasing until the

minimum in temperature variability close to the inversion height ($\sigma_{\min} = 6.1^{\circ}\text{C}$ at 145 m) and increasing above ($\sigma = 7.4^{\circ}\text{C}$ above 200 m). Although MAR underestimates the temperature variability over the entire profile by -29.05% compared to observations, it reproduces a sharp increase in temperature variability with height of -0.04°C/m between 5 and 160 m, comparable to the observed decrease in variability of -0.028°C/m between 15 and 145 m. ERA-5 does not show increased variability below the top of the inversion layer, likely due to a vertical resolution that does not capture the dynamics of a surface boundary layer. Additional model differences may arise from temporal resolution, where MAR is hourly, and ERA-5 is reported in 6-hr intervals.

When comparing directly with the UAS measurements, ERA-5 has a 25%–30% lower root-mean-square error (RMSE) than MAR for all variables (Figure 2). This may be expected as ERA-5 assimilates observations (at Summit, Greenland) in comparison to MAR, which uses ERA-5 forcing as lateral boundary conditions. Increasing the vertical resolution in MAR_hr reduces the RMSE by 5% for temperature and 6% for relative humidity, implying an increase in accuracy, although the RMSE is still larger than in ERA-5. A further expansive listing of statistics can be found in Table B2. An example of a reduced RMSE through the increase in vertical resolution can be seen on the seventh of July (Figure B1), where MAR_hr is able to capture the different humidity layers better than MAR and ERA-5. Here, the UAS measurements show a temperature inversion at ~ 200 m, which is also present in the 1 m binned profile, and which both MAR and MAR_hr capture.

Next, we evaluate the ability for MAR to determine temperature and humidity for all periods of observation, potentially demonstrating atmospheric states poorly represented in the model. Figure 4 shows that MAR is able to simulate the temporal evolution of the temperature well during the observational period. The specific humidity is captured well in most but not all of the observational period. Exceptions are the periods between 6/25 and 6/27 where MAR is too moist in the lower 500 m and between 7/5 and 7/6 when MAR produces too low humidity values in the lower 500 m. Notably, 6/25–6/27 includes several precipitation events, though it is not clear the connection these periods may have to inaccurate MAR model predictions. Overall, the MAR model represents the atmospheric state at EGRIP well during the summer period, especially when using MAR_hr.

3.4. HySPLIT-SWIM

We provide a model realization of water-vapor isotopes to evaluate assumptions about poleward vapor transport using a back trajectory model (HySPLIT) coupled to isotope-enabled water-distillation model (SWIM). The 1,920 modeled 10-day back-trajectories are shown in map view in Figure 8a, and latitude-altitude cross section in Figure 8b. Each individual trajectory is colored by the arrival height, indicated by the color bar and large closed circles in panel b). Several features of the air-parcel pathways are evident from these results. Air parcels arriving at higher altitudes have a broader spatial distribution and on average originate from lower latitudes than air parcels arriving at lower altitudes. This is broadly consistent with pseudo-adiabatic cooling of air as it is transported upward and pole-ward, and a moist-isentropic framework for poleward moisture transport (Bailey et al., 2019). The range of altitudes experienced by individual air parcels extends higher than the arrival point, consistent with subsidence over the site generally.

Isotopic results from HySPLIT-SWIM are shown in Figure 9. The two initial temperature conditions for air parcels, using the hottest temperature along the trajectory or the last time the air parcel was below the marine boundary layer, were effectively equivalent. Instead, we show the three cases for end temperature, described in Section 2.7. The model result v3, coldest temperature with adiabatic adjustment, demonstrates the closest match (mean difference of 0.84‰ $\delta^{18}\text{O}$ above 200 m) to observations, but deviates from observations below 200 m. The necessity of the adiabatic adjustment to match observations above the top of the inversion indicates that not enough water was removed during the trajectory of the water parcel in SWIM. Above the inversion layer, the relationship between water-vapor isotope depletion and altitude remains the same for all choices of temperature initializations in HySPLIT-SWIM as well as observations.

4. Discussion

There were two specific goals of this study that we sought to achieve. First, we aimed to deploy an Uncrewed Aerial System (UAS) fixed-wing drone platform to the top of the Greenland ice sheet, and then operate that system for a full summer field season in an extreme weather environment. We achieved this goal by completing

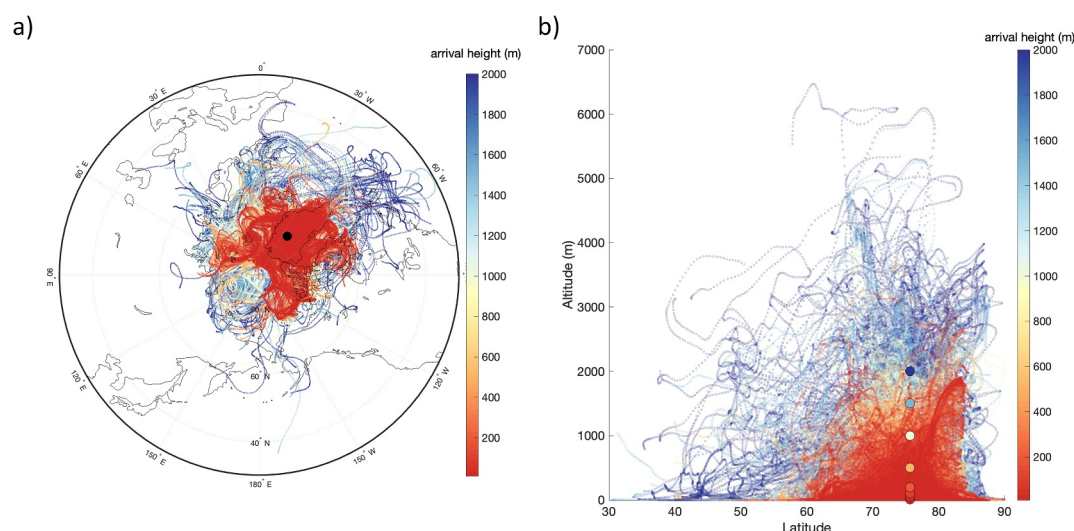


Figure 8. HySPLIT 10-day back-trajectory results. (a) All individual trajectories are shown, colored by arrival height, shown in the colorbar to the right. EGRIP site marked with black closed circle. (b) All trajectories shown in latitude-altitude cross section, colored by arrival height. Arrival locations marked with colored close circles.

104 flight missions over 34 days, with as many as 11 flights in a single day. On some days, we were unable to fly due to weather conditions and since the uncrewed aircraft is vulnerable to riming, our data set is biased toward clear-sky regimes or days where clouds existed above 200 m. Clouds over Northern Greenland peak in occurrence during JJA from the surface to 800–1,000 m (Lacour et al., 2017), and the cloud layer has typically slightly increased temperatures. To our knowledge, this is the first data set that provides detailed atmospheric profiles of water isotopes and the meteorological conditions (temperature, humidity) up to 1,500 m from interior Greenland or any polar ice sheet. Second, with the data set we have recovered, we aimed to compare those results to simple hydrologic and distillation models as an initial test of model physics. Our modeling approach was to target differing layers of the atmosphere (i.e., the structure of the atmosphere), which we identified as a near surface layer (0–2 m), a persistent inversion layer (~2 to ~200 m), and a layer from ~200 m to as high as 1,500 m. This study is not meant as a thorough test of model skill, but rather an initial indication of where model improvements may be needed. This sets the stage for future measurements and modeling analyses.

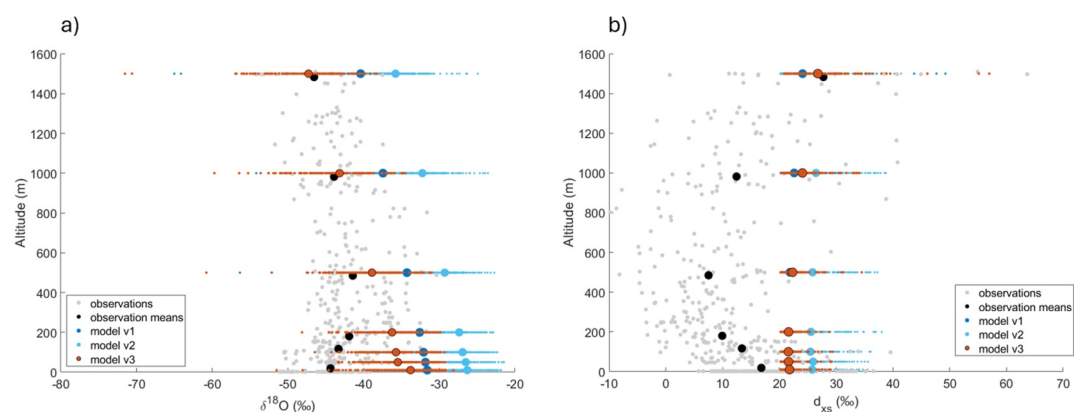


Figure 9. HySPLIT-SWIM model results compared to observations. Observations are denoted in gray. In orange, blue, and light blue we test three different final temperatures for traversing moist air parcels: (v1) the coldest temperature along the trajectory, (v2) arrival temperature in the back trajectory, and (v3) adiabatically cooled to match relative humidity observations. In all cases, the air parcel was initialized with the warmest temperature along the trajectory. Average for each model result and observations are shown as larger dots. In (a) we show results for $\delta^{18}\text{O}$ and in (b) we show δx_s .

4.1. Boundary Layer Structure

Our observations of the atmosphere above the Greenland interior ice sheet site are consistent with findings about inversions and katabatic winds over Greenland (Moore et al., 2013; Schwerdtfeger, 1972) and the Antarctic Ice Sheet (Grazioli et al., 2017; Hudson & Brandt, 2005; Schwerdtfeger, 1984). A strong surface-based temperature inversion, which occurs often during relatively dark or quiescent periods, decouples the boundary layer from the surface. The absolute humidity of inversion layer air remains low due to the influence of the cold ice sheet surface. Under inversion conditions, density-driven downslope flow is induced near the surface due to upslope radiative cooling, which we adopt as our working definition of a katabatic wind. This is connected to jet flow, or geostrophic flow, likewise informed by topography and horizontal temperature gradients over a large slope. These winds experience an Ekman spiral as the influence of surface friction decreases with height from the Coriolis force. As near-surface air masses flow downslope, they are subject to adiabatic warming reducing relative humidity (Grazioli et al., 2017). This aligns with the observed UAS profiles of the relative humidity (Figure 2c), and is much clearer in some individual profiles such as shown in flight “0003” (Appendix B). A reminder here that our operational bias is toward clear sky conditions, but not all conditions would be considered ‘inversion’ conditions due to scatter cloud cover or solar heating of the surface. In fact, near solar noon, solar surface heating induces mild convective mixing, contributing sublimated vapor to the boundary layer, and disrupting the near-surface inversion winds and katabatic flow/jet flow aloft set up during the previous night. We did not have reliable wind observations during profiling, making it difficult to concretely demonstrate the presence of an inversion wind, Ekman spiraling, or strong jet flow aloft during the observational period. However, MAR, MAR_hr, and ERA5 predict katabatic winds are strongest at ~250 m (Figure B2) consistent with predicted jet flow at this elevation on the ice sheet (Moore et al., 2013). There is some observational evidence for katabatic winds, evident in horizontal 2 m surface winds that were highly directionally consistent, originating upslope (Figure 1b). Accurate horizontal and vertical wind profiles to resolve katabatic winds at interior ice sheet sites by fixed-wing UAS should be of high priority in future studies.

4.2. Isotope Structure

For the full summer season and all UAS flights, the mean $\delta^{18}\text{O}$ and δD profiles show a clear pattern we detail in Section 3.3 and Figure 3 as an “inverse C-shape” that peaks around the temperature inversion at ~200 m, stays nearly constant up ~850 m, and then decreases up to ~1,500 m. The δxs profile shows the inverse behavior with a more pronounced “forward C-shape”. The $\delta^{18}\text{O}$ and δD “inverse C-shape” patterns are, on average, present under cloudy days (clouds >1,500 m), but much less pronounced or absent under clear sky conditions. For δxs , the “forward C-shape” is present under both conditions (cloudy and clear sky).

How can the patterns of the water isotopes in the atmosphere be explained? In this Section 4.2, we attempt to explain the patterns conceptually, and in Section 4.3 we utilize the SWIM model to further scrutinize the pattern. Ultimately, we find that several aspects of the water-isotope patterns require further study, and importantly, require improved model physics.

The conceptual explanation of $\delta^{18}\text{O}$ and δD can be separated into two parts: cloudy and clear sky. Because clouds influence both longwave and shortwave radiation, they can alter the surface conditions for vapor deposition or sublimation. For flights where clouds existed above 1500 m, the upper part of the inverse C-shape above the inversion height (200–850 m) exhibits more negative $\delta^{18}\text{O}$ and δD with increasing height in the atmosphere (Figure 3). This pattern relates to synoptic moisture input that has experienced some distillation process. For the vapor at higher altitudes (with more negative $\delta^{18}\text{O}$ and δD values), it is likely that the vapor had to start higher in the atmosphere at the moisture source to make it to higher atmospheric heights over Greenland (Figure 8). Conversely, vapor that started lower in the atmosphere at its moisture source tends to end up at lower altitudes over interior Greenland. However, this explanation cannot explain the lower part of the inverse C-shape, where $\delta^{18}\text{O}$ and δD are more negative with decreasing height in the atmosphere. In this case, as other researchers have noted (Kopeck et al., 2022; Wahl et al., 2022), sublimation at the ice sheet surface is likely a source of isotopically depleted water vapor into the atmosphere. Our results suggest that this vapor then mixes up to the inversion ceiling under inversion conditions. Under clear sky days, the inverse C-shape is barely evident in $\delta^{18}\text{O}$ and δD . Sublimation is still occurring, but now there is a larger energy input from direct shortwave radiation, warming the surface compared to cloudy days, which destabilizes the atmosphere and causes enhanced mixing effects, hence

rather constant $\delta^{18}\text{O}$ and δD profiles with height. It is important to note that, under both cloudy and clear sky days, the $\delta^{18}\text{O}$ and δD values have roughly the same values in the lowest few tens of meters of the atmosphere, as we argue, due to sublimation of water molecules from the ice sheet.

The isotope profiles substantially vary for different weather regimes (Figure B4), supporting the concept of moisture injection as a main driver of the isotopic composition of atmospheric water vapor. One noticeable exception to the seasonal average curve shape with a high density of measurement is the last period, VII. During this period, both observations and MAR show the driest boundary layer of the season. As the observed isotope values in this period match 2 m surface vapor isotope composition in the whole observed atmospheric column, the boundary layer may be well mixed with sublimated surface vapor in drier periods without synoptic moisture input.

The d_{xs} signal is often considered to be a proxy for SST, humidity, or wind speed at the moisture source origin. More generally though, d_{xs} can be thought of as representing the total amount of kinetic fractionation a vapor parcel has experienced (Merlivat & Jouzel, 1979). Our conceptual explanation of d_{xs} is consistent with our interpretations of the $\delta^{18}\text{O}$ and δD profiles. First, the exceedingly positive values of d_{xs} from 20 to 40 ‰ in the lower 10s of meters of the atmosphere for both clear and cloudy days is likely indicative of sublimation, a process that has been observed in the surface and sub-surface snow at EGRIP (Town et al., 2024; Wahl et al., 2021; Zühr et al., 2023). Qualitatively, d_{xs} will be higher in sublimated vapor due to the strong kinetic mass preference toward sublimation of lighter isotopes in sub-saturated air (Wahl et al., 2021). The fact that the forward C-shape is evident in d_{xs} on both clear and cloudy days suggests that increased mixing on clear days (as we also argue above for $\delta^{18}\text{O}$ and δD) is not strong enough to overcome the strong imprint of kinetic fractionation due to the sublimation process. However, the fact that d_{xs} on clear days is less concave (exhibits less of a C-shape) does indicate some mixing is still occurring. Above the inversion (200 m), d_{xs} increases with altitude. If, as we argue above, vapor at higher altitudes had to start higher in the atmosphere at the moisture source, then the d_{xs} will likely have a strong imprint of moisture source SSTs or relative humidity. Moisture from higher layers in the atmosphere often originates in lower latitudes where the strong solar incoming radiation triggers convection and mixes moisture into higher layers. In this case, the SSTs at lower latitudes would be warmer than SSTs at mid-to-high latitudes where less intense convection occurs. Thus, this is consistent with our arguments, vapor higher in the atmosphere over EGRIP on average started at higher altitudes at the moisture source, which would argue for a lower latitude moisture source (warmer SSTs) where convection is stronger, sending vapor into the high troposphere, resulting in longer travel distances for air parcels. This would result in more negative $\delta^{18}\text{O}$ and δD (more distillation over the transport path) and more positive d_{xs} values from warmer SSTs at lower latitude moisture sources. Furthermore, the standard deviation of d_{xs} at a given height increases above 850 m in altitude. This is likely the result of a larger source area of synoptic moisture input across the Atlantic mixing with the free atmosphere, with a wider range of d_{xs} values relating to moisture source conditions.

There are additional kinetic fractionation effects that may have affected the d_{xs} of vapor. One such effect could result from clear-sky deposition, or the saturation of vapor over ice. However, we find that measurements saturated with respect to ice were uncommon for observations, as flights were not conducted during any precipitation, and thus did not contribute to any trend (orange diamonds, Figure 3). Another source of kinetic fractionation may occur from phase changes within a mixed-phase cloud post-evaporation but pre-precipitation. Post-evaporative effects on d_{xs} may be small in our case, as liquid clouds seem to dominate cloud cover during summer over Greenland (Lacour et al., 2017). These air masses will have a d_{xs} signal more representative of SST, due to the smaller amount of kinetic exchange found in mixed-phase clouds (Jouzel & Merlivat, 1984).

4.3. Model Realizations of Atmospheric Water-Isotope Structure With HySPLIT-SWIM

Next, we utilize the HySPLIT-SWIM model to further clarify our understanding of water isotope profiles at the EGRIP site. HySPLIT-SWIM was able to recreate the pattern of the observed $\delta^{18}\text{O}$ and δD isotopic profile above the temperature inversion ceiling (200 m), with decreasing isotope values with increasing altitude, except that the model was offset from observations by about 6.58‰ $\delta^{18}\text{O}$ in model v1 and by about 11.52‰ in model v2, compared to 0.84‰ above 200 m in model v3 (Figure 9). The relationship between water-vapor isotopes and altitude remains fixed across all vapor initialization schemes (v1, v2, v3) that affect the magnitude of temperature gradient experienced by the parcel along its trajectory. This implies that, on average, the relative amount of

fractionation as a function of arrival altitude is a conversed quantity across different temperature gradients within the default fractionation configuration in SWIM. A downward slope is expected, as water isotopes are generally depleted linearly with relation to total heat along its trajectory and thus follows an isotopic lapse rate (5.8–6.5‰/km, $\delta^{18}\text{O}$) upon arrival to EGRIP.

When moisture is removed in the model to match relative-humidity observations at EGRIP (model configuration v3, Section 2.7), HySPLIT-SWIM was able to recreate the water-vapor isotopic profile with no significant offset above the temperature inversion. This implies that, to first order, the δD and $\delta^{18}\text{O}$ isotopic pattern of water vapor above the inversion at EGRIP was well-represented by the model's fractionation physics and representation of large-scale moisture transport, but poorly represented in the precipitation scheme, which underestimated water removal along transport pathways. Moisture is removed in SWIM when an air parcel reaches a specific level of supersaturation tuned from precipitation observations (Markle & Steig, 2022). This parameterization has not been tested prior to this study in the vapor phase across the temperature range a water parcel may experience on its way to Greenland. Supersaturation tuning derived from an aerial record of water-vapor isotopes should be a target for future studies investigating this precipitation discrepancy.

The match between SWIM and observations in model configuration v3 breaks down below the temperature inversion height at 200 m. Within the inversion, HySPLIT-SWIM follows the isotopic lapse rate and continues to predict increasing δD and $\delta^{18}\text{O}$ isotope values with decreasing altitude, whereas observations reveal decreasing isotope values with decreasing altitude (i.e., the lower part of the inverse C-shape). Note that HySPLIT-SWIM does not include evaporative recharge or surface effects for air parcels along their transport pathways and consequently cannot capture sublimated vapor from the ice sheet mixing upwards, which we propose results in the disagreement between model and observations below the inversion. Dietrich et al. (2024) found that EGRIP has a strong sublimation flux (~31% of deposition) leaving the ice sheet during the 2016–2019 summers. Another unknown factor is the impact from moisture input of gravity-driven katabatic winds, whose upslope moisture source conditions would be consistent with a depleted (i.e., colder) vapor source. This impact would be magnified after solar noon due to a decreasing residual layer, which would flush local sublimated vapor downslope, just as upslope vapor is received. To estimate the relative amount of contribution of katabatic winds in future studies, water-vapor isotope profiles would need to be retrieved from a location without them, such as from Summit area of the Greenlandic ice divide.

HySPLIT-SWIM is unable to recreate the pattern of dxs with height, although the general magnitude of dxs values in the atmospheric column is about the same as observations (Figure 9). The inability to reproduce the distinct “forward C-shape” in the dxs profile is most likely a results of missing surface effects that are not mixed into the surface near vapor along its transport pathway in HYSPLIT-SWIM. Like observations, HySPLIT-SWIM does exhibit larger dxs variability at higher altitudes, likely the result of a larger source area of synoptic moisture input across the Atlantic. In fact, HySPLIT back trajectories reveal a broader catchment of moisture sources as a function of altitude (Figure 8), which could result in larger dxs variability at higher altitudes due to more diverse kinetic fractionation conditions across a more diverse set of moisture sources. Greenland has been modeled in summer to show input of moisture from various North Atlantic sources and the EGRIP field site is located at the intersection of these, having similar moisture inputs from a diverse set of locations across the Northern Atlantic (Nusbaumer et al., 2019).

5. Conclusion and Future Outlook

Most water isotope-enabled hydrologic models are benchmarked with either source water (from the ocean) or the end-product precipitation, in our case snow over the ice sheet. There is a substantial missing part of the story—what happens between source and sink, and are models capable of modeling fractionation associated with vapor transport at intermediate steps? Our project goal was to utilize fixed-wing drones to obtain data that provides info about water-vapor isotopes and meteorology over the Greenland Ice Sheet, to further refine the physics of isotope-enabled models.

We present a record of atmospheric water-vapor isotopes and meteorological variables (temperature and humidity) for 104 drone flights occurring across a summer season at the EGRIP ice core camp in interior northeast Greenland. Depending on weather conditions and flight safety considerations, we achieved up to 11 flights per day, as high as 1,500 m in the atmosphere. To our knowledge, this is the first such data set of its kind, novel for both the resolution

of atmospheric profile measurements (many times per day) and for accessing lower parts of the atmosphere (below and within the planetary boundary layer) at a high vertical resolution. Additionally, as a constraint for modeling, we collected snow samples from the ice sheet surface at 12-hr intervals at depths of 1 and 5 cm.

Based upon the vertical atmospheric drone profiles, we find that day-to-day variability of water isotopes in the atmosphere is noisy and may vary for many different reasons. However, when water isotopes are averaged across the summer season in vertical bins of 50 m, there is clear structure that emerges. For δD and $\delta^{18}O$ 50 m bins, we observe an increase with height up to ~ 200 m which is both a temperature and isotopic inversion layer. Then we observe a layer with variable values from 200 to 850 m, and a decrease with height above 850 m; this forms an “inverse C-shape”. Inversely, the binned dxs is high close to the surface, decreases with height up to approximately 200 m, is nearly constant between 200 and 850 m, and increases above 850 m, forming a “forward C-shape”. Attempts to model this structure reveal shortcomings in the physics of simple distillation models coupled with back trajectories.

We run a 10-day back-trajectory model for each observed drone profile with the Hybrid Single-Particle Lagrangian Integrated Trajectory model (HySPLIT) coupled to a water-isotope distillation model, the Simple Water Isotope Model (SWIM), constrained by NCEP reanalysis data. With HySPLIT-SWIM, we can evaluate the assumptions traditionally made in models used to predict the isotopic composition of precipitation, but now also with vapor-phase observations in the atmosphere above the ice sheet. We find that HySPLIT-SWIM is somewhat successful in recreating the isotopic structure of the atmosphere, except for two key aspects: (a) For δD and $\delta^{18}O$, the model cannot recreate the bottom of the inverse C-shape structure in the lowest 200 m of the atmosphere within the mean-inversion layer, and (b) For δD and $\delta^{18}O$, the model results are too heavy by a number of per mille, indicating that not enough “rain out” occurs along the vapor transport pathways. The model is unable to model dxs well.

We present an argument as to why the inverse and forward C-shapes exist for δD , $\delta^{18}O$, and dxs , that is, why do isotopic values below ~ 200 m tend to get lighter (more depleted in the heavier δD and $\delta^{18}O$ isotopes) approaching the ice sheet surface, and inversely for dxs , why do values become more positive. We find that this is likely due to net sublimation flux from the ice sheet surface, which mixes upwards. This result is in line with prior small-tower (2 m height) results at EGRIP that show a strong upward flux of sublimated vapor from the ice sheet surface during summer (Dietrich et al., 2024). The HySPLIT-SWIM model cannot accurately simulate this sublimation as it does not include interactions between the ice sheet and atmosphere, including sublimation. This represents an important target for model improvement. Similarly, the model's failure to approximate the full extent of rainout, that is, the full extent of distillation of heavy isotopes in the atmosphere, is another consideration for improved model physics.

Since the EGRIP site has a persistent katabatic wind that may confound our results, we aim to make future drone measurements at the Greenland ice divide. The ice divide would be free of katabatic winds, with the added benefit of capturing air parcels from a much wider geographic extent than EGRIP. Two potential sites of interest would be Summit Station (U.S.) or the GRIP site (European). Within such a campaign, the operational filter for flights may be relaxed with the addition of greater crew numbers, enabling nighttime flights. Additionally, a longer duration of deployment combined with opportunities for automation in sampling procedures will allow for a greater breadth of seasonal coverage at a higher density of flights. We will include an airborne wind sensor, needed both for careful consideration of katabatic winds and as an additional model-observation comparison. It remains an engineering hurdle to allow for flights during riming conditions and precipitation events. The development of UAS vehicles of the same class used in this study that can fly in these conditions should be a priority.

Appendix A: Calibration

The CRDS has differing isotopic responses at different levels of specific humidity. Suites of measurements were made to characterize this response described in Rozmiarek et al. (2021). Standard calibrations in this way were performed for the CRDS instrument used for UAS flask system analysis. For each of the four standards, a range of 500 to 25,000 ppm water vapor was produced by a nebulizer and flash vaporized by a furnace before getting introduced into the CRDS instrument. Ranges of humidities were produced by introducing a controlled dry air dilution after nebulization. The standards, their values, and uncertainties can be found in A1. Additional details on the calibration scheme can be found in Jones et al. (2017) (Table A1).

Table A1

Tracing of Uncertainties Is Provided for Primary Reference Water Standards () and Secondary Water Standards Developed, Which are Reported in Units of per Mille*

Standard	δD (‰)	δD uncertainty	$\delta^{18}O$ (‰)	$\delta^{18}O$ uncertainty
VSMOW2*	0	0.3	0	0.02
SLAP2*	−427.5	0.3	−55.5	0.02
GISP*	−189.5	1.2	−24.76	0.09
BSW	−111.65	0.2 (1.3)	−14.15	0.02 (0.10)
ASW	−239.13	0.3 (1.3)	−30.30	0.04 (0.10)
PSW	−355.18	0.2 (1.3)	−45.41	0.05 (0.11)
SPGSW	−434.47	0.2 (1.3)	−55.18	0.05 (0.11)

Note. The four secondary standards (BSW, ASW, PSW, and SPGSW) are previously calibrated in the laboratory and are defined relative to the primary standards (VSMOW2, SLAP2, and GISP) on which values and uncertainty are reported by the IAEA. Secondary standards are reported with uncertainty determined across multiple IRMS and CRDS platforms. In parentheses are the combined uncertainty of both the primary and secondary standard tie added in quadrature.

Appendix B: Additional Supporting Figures and Tables

Figure B1

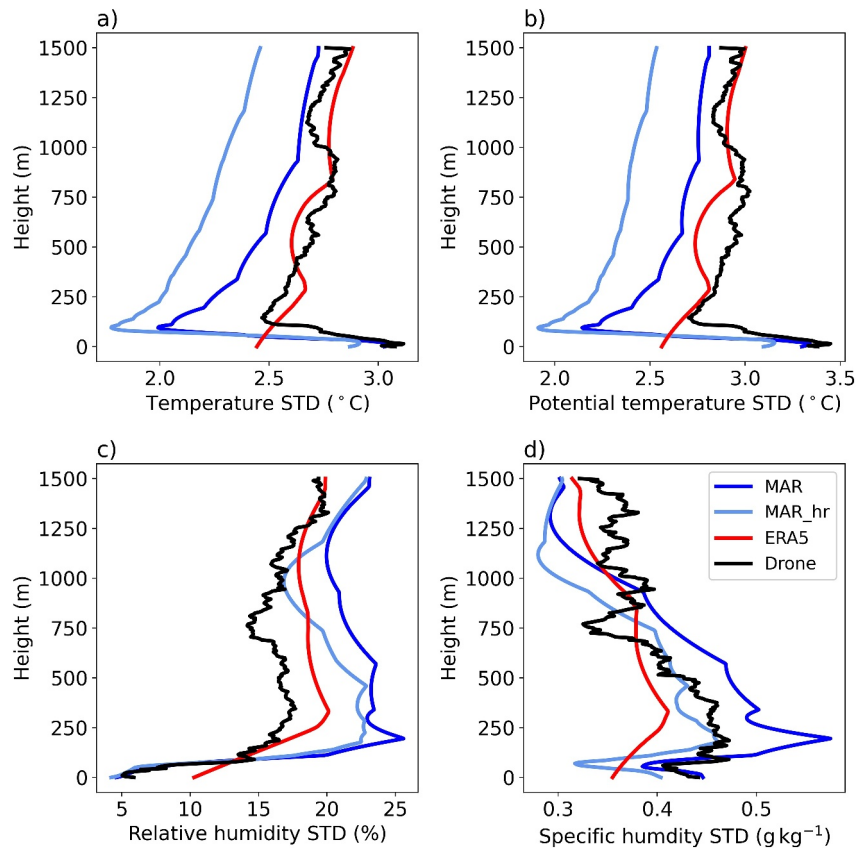


Figure B1. Vertical profiles of the first standard deviation of (a) temperature, (b) potential temperature, (c) relative humidity, and (d) specific humidity across 104 flights as measured by the UAS (black) and simulated by MAR (blue), MAR_hr (light blue) and ERA5 (red).

Figure B2

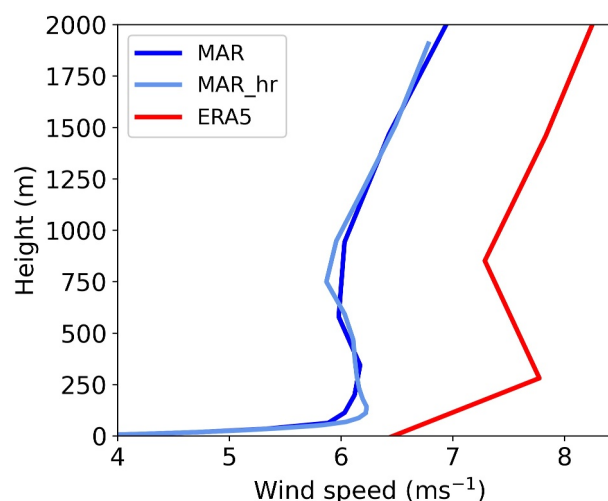


Figure B2. Average wind speed profile simulation in MAR for the sampling period at a lower vertical resolution of 24 layers (dark blue) and a higher vertical resolution of 40 layers (light blue), and in the ERA-5 reanalysis product (red). All three models show a katabatic wind layer sign above the surface boundary layer up to 750 m.

Figure B3

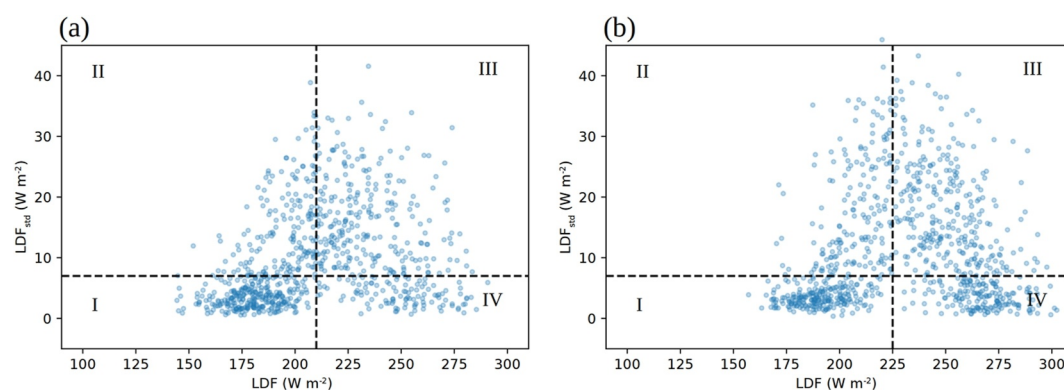


Figure B3. Scatterplots of 6-hourly mean versus standard deviation of hourly longwave downwelling fluxes from the PROMICE AWS near EastGRIP for 2016–2022. Panel (a) shows June data, panel (b) shows July data. Thresholds used in combination to filter for cloud presence are shown as dashed lines. Quadrant I are considered clear sky 6-hourly periods, all quadrants represent cloudy 6-hourly periods.

Figure B4

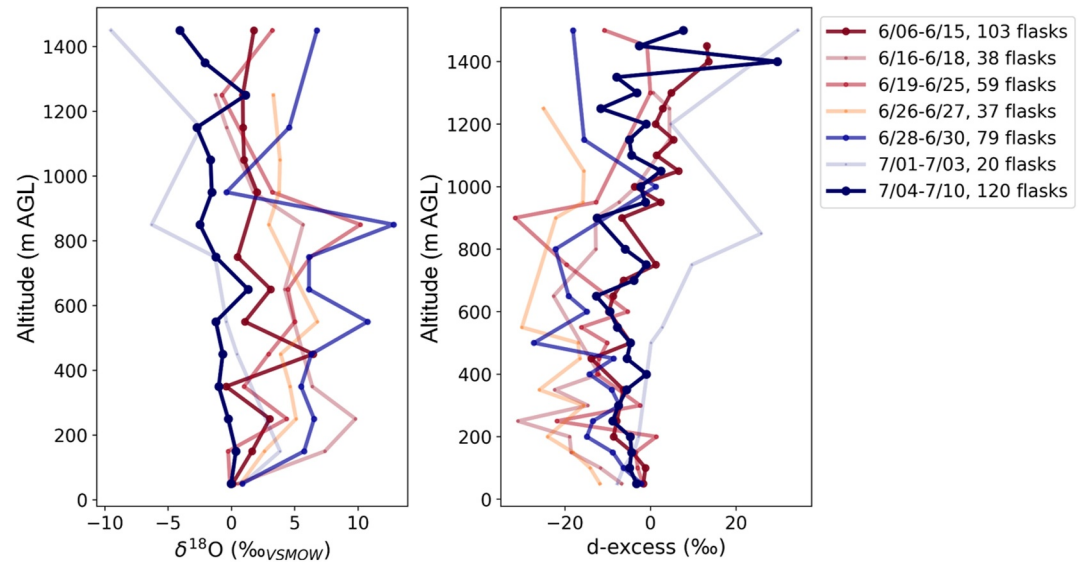


Figure B4. Isotope profiles in $\delta^{18}\text{O}$ and d_{ex} for each measurement period in 50 m bins. Opacity of line and size of dots determined by number of observations in measurement period.

Figure B5

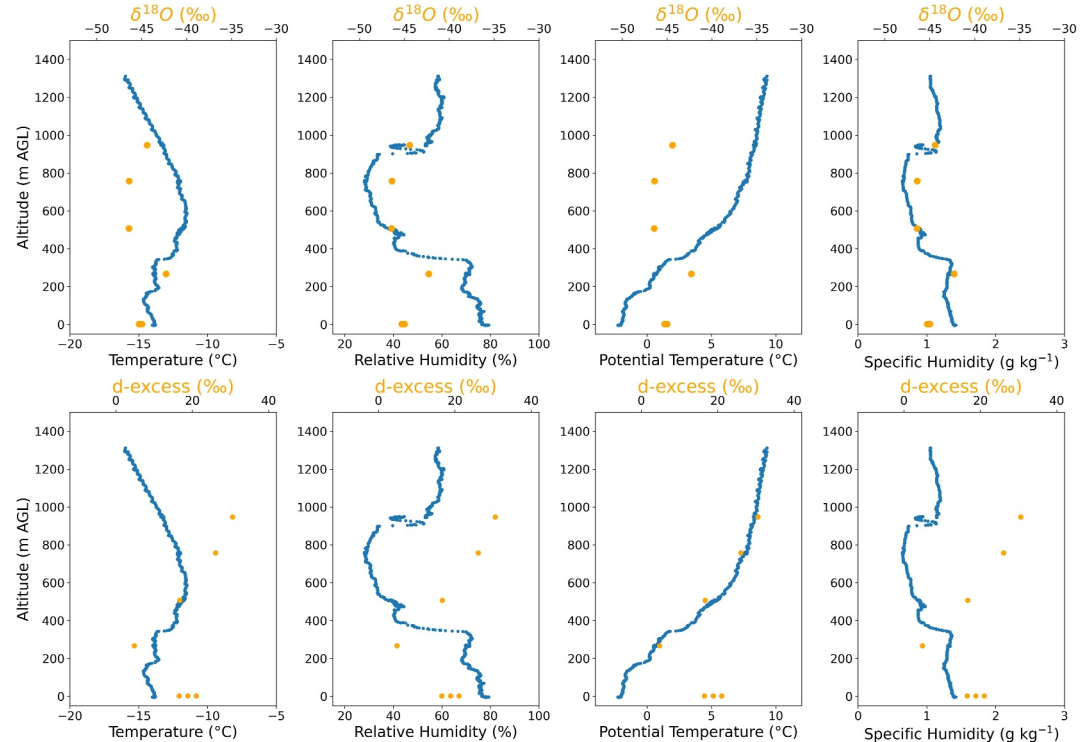


Figure B5. Case study flight, flight 0003, flown 07 June 2022 beginning at 14:15 local time. In blue are atmospheric state variables (1) temperature ($^{\circ}\text{C}$), (2) relative humidity (%) with respect to water, (3) potential temperature ($^{\circ}\text{C}$), and (4) specific humidity (g/kg). In orange are air capture measurements by UAS and surface measurements at 2 m. In the top row of subplots is $\delta^{18}\text{O}(\text{‰})$ and in the bottom row is $d\text{-excess}(\text{‰})$.

Table B1

Table B1 Time Periods of Isotopic Observations During the Sampling Period Determined by Expert Opinion			
Region	Time period	Number of isotopic observations	Distinct features
I	6/06–6/15	103	Beginning through first sampling gap due to weather conditions
II	6/16–6/18	38	Next fair weather period with isotopically distinct precipitation events
III	6/19–6/25	59	Next poor weather period with many precipitation events
IV	6/26–6/27	37	Air mass with distinct specific humidity
V	6/28–6/30	79	Shift toward higher specific humidity and isotopic signature
VI	7/01–7/03	20	Air mass with distinct specific humidity above near-surface PBL
VII	7/04–7/31	120	Break in observations due to weather followed by distinct isotopic signal

Note. Periods are determined and justified in the distinct features column. Number of isotopic observations correspond to individual flasks, not specific heights which may contain flask pairs.

Table B2

Table B2 Additional Statistics Between UAS Meteorological Profiles, MAR, and ERA-5				
	St dev	Bias	Correlation	RMSE
	Obs, MAR, ERA-5	MAR, ERA-5	MAR, ERA-5	MAR, ERA-5
T (°C)	3.30, 3.04, 3.07	0.10, −0.42	0.86, 0.92	1.72, 1.37
θ (°C)	4.05, 3.67, 3.97	0.59, −0.14	0.88, 0.93	2.03, 1.48
q ($\frac{g}{kg}$)	0.44, 0.48, 0.37	−0.04, −0.12	0.62, 0.76	0.41, 0.31
RH (%)	16.59, 22.07, 18.42,	5.72, 5.23	0.52, 0.70	20.43, 14.61

Note. Listed are temperature (T), potential temperature (θ), specific humidity (q), and relative humidity (RH). We compute the first standard deviation for all data for all flights and both model realizations. Additionally, we present difference or bias, cross-correlation, and root mean square error for all profiles up to their flight ceiling compared against observations. All models are computed for the time periods of flight missions during the sampling period, not for the full duration of the sampling period.

Data Availability Statement

Data for this study (observations, MAR, and SWIM model results) are available at the Arctic Data Center (Rozmiarek et al., 2025). The Arctic Data Center is committed to providing citable data sets to facilitate reproducible science. Each DOI issued by the Arctic Data Center is intended to represent a unique, immutable version of a data package.

References

- Akers, P. D., Kopec, B. G., Mattingly, K. S., Klein, E. S., Causey, D., & Welker, J. M. (2020). Baffin bay sea ice extent and synoptic moisture transport drive water vapor isotope (δ 18 o, δ 2 h, and deuterium excess) variability in coastal northwest Greenland. *Atmospheric Chemistry and Physics*, 20(22), 13929–13955. <https://doi.org/10.5194/acp-20-13929-2020>
- Allan, R. P., Barlow, M., Byrne, M. P., Cherchi, A., Douville, H., Fowler, H. J., et al. (2020). Advances in understanding large-scale responses of the water cycle to climate change. *Annals of the New York Academy of Sciences*, 1472(1), 49–75. <https://doi.org/10.1111/nyas.14337>
- Bailey, A., Singh, H. K., & Nusbaumer, J. (2019). Evaluating a moist isentropic framework for poleward moisture transport: Implications for water isotopes over Antarctica. *Geophysical Research Letters*, 46(13), 7819–7827. <https://doi.org/10.1029/2019gl082965>
- Boisvert, L. N., Lee, J. N., Lenaerts, J. T., Noël, B., Van Den Broeke, M. R., & Nolin, A. W. (2017). Using remotely sensed data from airs to estimate the vapor flux on the Greenland ice sheet: Comparisons with observations and a regional climate model. *Journal of Geophysical Research: Atmospheres*, 122(1), 202–229. <https://doi.org/10.1002/2016jd025674>
- Bony, S., Risi, C., & Vimeux, F. (2008). Influence of convective processes on the isotopic composition (δ 18o and δ d) of precipitation and water vapor in the tropics: 1. Radiative-convective equilibrium and tropical ocean–global atmosphere–coupled ocean–atmosphere response experiment (toga-coare) simulations. *Journal of Geophysical Research*, 113(D19). <https://doi.org/10.1029/2008jd009942>

Acknowledgments

The authors are grateful for the funding provided by the National Science Foundation award 1833165, “Closing the Water Vapor Exchange Budget Between the Ice Sheets and Free Atmosphere”, managed by Jennifer Mercer. We wish to thank Dorthe Dahl-Jensen, University of Copenhagen, and the EastGRIP international team for their support of the fieldwork on the Greenland Ice Sheet; EastGRIP is directed and organized by the Centre for Ice and Climate at the Niels Bohr Institute, University of Copenhagen. It is supported by funding agencies and institutions in Denmark (A. P. Møller Foundation, University of Copenhagen), the USA (US National Science Foundation, Office of Polar Programs), Germany (Alfred Wegener Institute, Helmholtz Centre for Polar and Marine Research), Japan (National Institute of Polar Research and Arctic Challenge for Sustainability), Norway (University of Bergen and Bergen Research Foundation), Switzerland (Swiss National Science Foundation), France (French Polar Institute Paul-Émile Victor, Institute for Geosciences and Environmental research), and China (Chinese Academy of Sciences and Beijing Normal University). This project received funding from the European Research Council (ERC) under the European Union's Horizon 2020 research and innovation program: Starting Grant-SNOWISO (Grant Agreement 759526). This work was funded in part by NSF Grant 2137083—Collaborative Research: NSFGEONERC: Integrated Characterization of Energy, Clouds, Atmospheric state, and Precipitation at Summit: Measurements along Lagrangian Transects. We thank the 109th Air National Guard for logistical support in reaching the remote EastGRIP ice core camp, the shipment of equipment, and for safe passage for our team members. UAS flight training and support provided by CU Division of Public Safety Flight Operations Department and Director of Flight Operations, Dan Hesselius. UAS expertise and design were provided by Jack Elston and the team at Black Swift Technologies. Nose cone design assistance provided by Dirk Richter, University of Colorado.

- Bowen, G. J., Cai, Z., Fiorella, R. P., & Putman, A. L. (2019). Isotopes in the water cycle: Regional-to global-scale patterns and applications. *Annual Review of Earth and Planetary Sciences*, 47(1), 453–479. <https://doi.org/10.1146/annurev-earth-053018-060220>
- Craig, H. (1961). Isotopic variations in meteoric waters. *Science*, 133(3465), 1702–1703. <https://doi.org/10.1126/science.133.3465.1702>
- Dansgaard, W. (1964). Stable isotopes in precipitation. *Tellus*, 16(4), 436–468. <https://doi.org/10.1111/j.2153-3490.1964.tb00181.x>
- Dee, S., Bailey, A., Conroy, J. L., Atwood, A., Stevenson, S., Nusbaumer, J., & Noone, D. (2023). Water isotopes, climate variability, and the hydrological cycle: Recent advances and new frontiers. *Environmental Research: Climate*, 2(2), 022002. <https://doi.org/10.1088/2752-5295/acb1>
- Dee, S. G., Nusbaumer, J., Bailey, A., Russell, J. M., Lee, J.-E., Konecky, B., et al. (2018). Tracking the strength of the walker circulation with stable isotopes in water vapor. *Journal of Geophysical Research: Atmospheres*, 123(14), 7254–7270. <https://doi.org/10.1029/2017jd027915>
- Dietrich, L. J., Steen-Larsen, H. C., Wahl, S., Faber, A.-K., & Fettweis, X. (2024). On the importance of the humidity flux for the surface mass balance in the accumulation zone of the Greenland ice sheet. *The Cryosphere*, 18(1), 289–305. <https://doi.org/10.5194/tc-18-289-2024>
- Dietrich, L. J., Steen-Larsen, H. C., Wahl, S., Jones, T. R., Town, M. S., & Werner, M. (2023). Snow-atmosphere humidity exchange at the ice sheet surface alters annual mean climate signals in ice core records. *Geophysical Research Letters*, 50(20), e2023GL104249. <https://doi.org/10.1029/2023gl104249>
- Draxler, R. R., & Hess, G. (1998). An overview of the hysplit_4 modelling system for trajectories. *Australian Meteorological Magazine*, 47(4), 295–308.
- Fausto, R. S., Van As, D., Mankoff, K. D., Vandecrux, B., Citterio, M., Ahlström, A. P., et al. (2021). Programme for monitoring of the Greenland ice sheet (promice) automatic weather station data. *Earth System Science Data*, 13(8), 3819–3845. <https://doi.org/10.5194/essd-13-3819-2021>
- Fettweis, X., Box, J. E., Agosta, C., Amory, C., Kittel, C., Lang, C., et al. (2017). Reconstructions of the 1900–2015 Greenland ice sheet surface mass balance using the regional climate mar model. *The Cryosphere*, 11(2), 1015–1033. <https://doi.org/10.5194/tc-11-1015-2017>
- Fettweis, X., Franco, B., Tedesco, M., Van Angelen, J., Lenaerts, J. T., Van Den Broeke, M. R., & Gallée, H. (2013). Estimating the Greenland ice sheet surface mass balance contribution to future sea level rise using the regional atmospheric climate model mar. *The Cryosphere*, 7(2), 469–489. <https://doi.org/10.5194/tc-7-469-2013>
- Fettweis, X., Gallée, H., Lefebvre, F., & Van Ypersele, J.-P. (2005). Greenland surface mass balance simulated by a regional climate model and comparison with satellite-derived data in 1990–1991. *Climate Dynamics*, 24(6), 623–640. <https://doi.org/10.1007/s00382-005-0010-y>
- Field, R. (2010). *Large-scale and microphysical controls on water isotopes in the atmosphere*. University of Toronto.
- Galewsky, J., & Hurley, J. V. (2010). An advection-condensation model for subtropical water vapor isotopic ratios. *Journal of Geophysical Research*, 115(D16). <https://doi.org/10.1029/2009jd013651>
- Galewsky, J., Steen-Larsen, H. C., Field, R. D., Worden, J., Risi, C., & Schneider, M. (2016). Stable isotopes in atmospheric water vapor and applications to the hydrologic cycle. *Reviews of Geophysics*, 54(4), 809–865. <https://doi.org/10.1002/2015rg000512>
- Gallée, H., & Schayes, G. (1994). Development of a three-dimensional meso- γ primitive equation model: Katabatic winds simulation in the area of terra nova bay, Antarctica. *Monthly Weather Review*, 122(4), 671–685. [https://doi.org/10.1175/1520-0493\(1994\)122<0671:doatdm>2.0.co;2](https://doi.org/10.1175/1520-0493(1994)122<0671:doatdm>2.0.co;2)
- Grazioli, J., Madeleine, J.-B., Gallée, H., Forbes, R. M., Genthon, C., Krinner, G., & Berne, A. (2017). Katabatic winds diminish precipitation contribution to the antarctic ice mass balance. *Proceedings of the National Academy of Sciences*, 114(41), 10858–10863. <https://doi.org/10.1073/pnas.1707633114>
- Henze, D., Noone, D., & Toohey, D. (2022). Aircraft measurements of water vapor heavy isotope ratios in the marine boundary layer and lower troposphere during oracles. *Earth System Science Data*, 14(4), 1811–1829. <https://doi.org/10.5194/essd-14-1811-2022>
- Hersbach, H., Bell, B., Berrisford, P., Hirahara, S., Horányi, A., Muñoz-Sabater, J., et al. (2020). The era5 global reanalysis. *Quarterly Journal of the Royal Meteorological Society*, 146(730), 1999–2049. <https://doi.org/10.1002/qj.3803>
- Hu, J., Bailey, A., Nusbaumer, J., Dee, S., Sasser, C., & Worden, J. (2022). Tracking shallow convective mixing and its influence on low-level clouds with stable water isotopes in vapor. *Journal of Geophysical Research: Atmospheres*, 127(5), e2021JD035355. <https://doi.org/10.1029/2021jd035355>
- Hudson, S. R., & Brandt, R. E. (2005). A look at the surface-based temperature inversion on the Antarctic plateau. *Journal of Climate*, 18(11), 1673–1696. <https://doi.org/10.1175/jcli3360.1>
- Hughes, A. G., Wahl, S., Jones, T. R., Zühr, A., Hörhold, M., White, J. W., & Steen-Larsen, H. C. (2021). The role of sublimation as a driver of climate signals in the water isotope content of surface snow: Laboratory and field experimental results. *The Cryosphere*, 15(10), 4949–4974. <https://doi.org/10.5194/tc-15-4949-2021>
- Jones, T., Cuffey, K., White, J., Steig, E., Buizert, C., Markle, B., et al. (2017). Water isotope diffusion in the wais divide ice core during the holocene and last glacial. *Journal of Geophysical Research: Earth Surface*, 122(1), 290–309. <https://doi.org/10.1002/2016j003938>
- Jouzel, J., Delaygue, G., Landais, A., Masson-Delmotte, V., Risi, C., & Vimeux, F. (2013). Water isotopes as tools to document oceanic sources of precipitation. *Water Resources Research*, 49(11), 7469–7486. <https://doi.org/10.1002/2013wr013508>
- Jouzel, J., & Merlivat, L. (1984). Deuterium and oxygen 18 in precipitation: Modeling of the isotopic effects during snow formation. *Journal of Geophysical Research*, 89(D7), 11749–11757. <https://doi.org/10.1029/jd089id07p11749>
- Klein, E. S., Cherry, J., Young, J., Noone, D., Leffler, A., & Welker, J. (2015). Arctic cyclone water vapor isotopes support past sea ice retreat recorded in Greenland ice. *Scientific Reports*, 5(1), 10295. <https://doi.org/10.1038/srep10295>
- Komuro, Y., Nakazawa, F., Hirabayashi, M., Goto-Azuma, K., Nagatsuka, N., Shigeyama, W., et al. (2021). Temporal and spatial variabilities in surface mass balance at the egrip site, Greenland from 2009 to 2017. *Polar Science*, 27, 100568. <https://doi.org/10.1016/j.polar.2020.100568>
- Kopec, B. G., Feng, X., Osterberg, E. C., & Posmentier, E. S. (2022). Climatological significance of δd - δ18o line slopes from precipitation, snow pits, and ice cores at summit, Greenland. *Journal of Geophysical Research: Atmospheres*, 127(21), e2022JD037037. <https://doi.org/10.1029/2022jd037037>
- Lacour, A., Chepfer, H., Shupe, M. D., Miller, N. B., Noel, V., Kay, J., et al. (2017). Greenland clouds observed in calipso-goccp: Comparison with ground-based summit observations. *Journal of Climate*, 30(15), 6065–6083. <https://doi.org/10.1175/jcli-d-16-0552.1>
- Leroy-Dos Santos, C., Masson-Delmotte, V., Casado, M., Fourré, E., Steen-Larsen, H., Maturilli, M., et al. (2020). A 4.5 year-long record of svalbard water vapor isotopic composition documents winter air mass origin. *Journal of Geophysical Research: Atmospheres*, 125(23), e2020JD032681. <https://doi.org/10.1029/2020jd032681>
- Markle, B. R., & Steig, E. J. (2022). Improving temperature reconstructions from ice-core water-isotope records. *Climate of the Past*, 18(6), 1321–1368. <https://doi.org/10.5194/cp-18-1321-2022>
- Merlivat, L., & Jouzel, J. (1979). Global climatic interpretation of the deuterium-oxygen 18 relationship for precipitation. *Journal of Geophysical Research*, 84(C8), 5029–5033. <https://doi.org/10.1029/jc084ic08p05029>
- Moore, G. W. K., Renfrew, I. A., & Cassano, J. J. (2013). Greenland plateau jets. *Tellus A: Dynamic Meteorology and Oceanography*, 65(1), 17468. <https://doi.org/10.3402/tellusa.v65i0.17468>

- Nakazawa, F., Nagatsuka, N., Hirabayashi, M., Goto-Azuma, K., Steffensen, J. P., & Dahl-Jensen, D. (2021). Variation in recent annual snow deposition and seasonality of snow chemistry at the east Greenland ice core project (egrip) camp, Greenland. *Polar Science*, 27, 100597. <https://doi.org/10.1016/j.polar.2020.100597>
- Newman, B., Tanweer, A., & Kurttaş, T. (2009). *Iaea standard operating procedure for the liquid-water stable isotope analyser*. IAEA Yayınları/ IAEA Publications.
- Nusbaumer, J., Alexander, P. M., LeGrande, A. N., & Tedesco, M. (2019). Spatial shift of Greenland moisture sources related to enhanced arctic warming. *Geophysical Research Letters*, 46(24), 14723–14731. <https://doi.org/10.1029/2019gl084633>
- Putman, A. L., Fiorella, R. P., Bowen, G. J., & Cai, Z. (2019). A global perspective on local meteoric water lines: Meta-analytic insight into fundamental controls and practical constraints. *Water Resources Research*, 55(8), 6896–6910. <https://doi.org/10.1029/2019wr025181>
- Risi, C., Müller, C., & Blossey, P. (2020). What controls the water vapor isotopic composition near the surface of tropical oceans? Results from an analytical model constrained by large-eddy simulations. *Journal of Advances in Modeling Earth Systems*, 12(8), e2020MS002106. <https://doi.org/10.1029/2020ms002106>
- Risi, C., Noone, D., Frankenberg, C., & Worden, J. (2013). Role of continental recycling in intraseasonal variations of continental moisture as deduced from model simulations and water vapor isotopic measurements. *Water Resources Research*, 49(7), 4136–4156. <https://doi.org/10.1002/wrcr.20312>
- Rozmiarek, K. S., Dietrich, L. J., Vaughn, B. H., Town, M. S., Markle, B. R., Morris, V., & Jones, T. R. (2025). Atmosphere to surface profiles of water vapor isotopes and meteorological conditions over the northeast Greenland ice sheet data product for 2022 field campaign [dataset]. *Arctic Data Center*. <https://doi.org/10.18739/A2QR4NS5C>
- Rozmiarek, K. S., Vaughn, B. H., Jones, T. R., Morris, V., Skorski, W. B., Hughes, A. G., et al. (2021). An unmanned aerial vehicle sampling platform for atmospheric water vapor isotopes in polar environments. *Atmospheric Measurement Techniques*, 14(11), 7045–7067. <https://doi.org/10.5194/amt-14-7045-2021>
- Salmon, O. E., Welp, L. R., Baldwin, M. E., Hajny, K. D., Stirm, B. H., & Shepson, P. B. (2019). Vertical profile observations of water vapor deuterium excess in the lower troposphere. *Atmospheric Chemistry and Physics*, 19(17), 11525–11543. <https://doi.org/10.5194/acp-19-11525-2019>
- Schauer, A. J., Schoenemann, S. W., & Steig, E. J. (2016). Routine high-precision analysis of triple water-isotope ratios using cavity ring-down spectroscopy. *Rapid Communications in Mass Spectrometry*, 30(18), 2059–2069. <https://doi.org/10.1002/rcm.7682>
- Schmidt, G. A., Hoffmann, G., Shindell, D. T., & Hu, Y. (2005). Modeling atmospheric stable water isotopes and the potential for constraining cloud processes and stratosphere-troposphere water exchange. *Journal of Geophysical Research*, 110(D21). <https://doi.org/10.1029/2005jd005790>
- Schwerdtfeger, W. (1972). The vertical variation of the wind through the friction-layer over the Greenland ice cap. *Tellus*, 24(1), 13–16. <https://doi.org/10.1111/j.2153-3490.1972.tb01528.x>
- Schwerdtfeger, W. (1984). *Weather and climate of the antarctic*. Elsevier.
- Sodemann, H., Aemisegger, F., Pfahl, S., Bitter, M., Corsmeier, U., Feuerle, T., et al. (2017). The stable isotopic composition of water vapour above corsica during the hymex sop1 campaign: Insight into vertical mixing processes from lower-tropospheric survey flights. *Atmospheric Chemistry and Physics*, 17(9), 6125–6151. <https://doi.org/10.5194/acp-17-6125-2017>
- Steen-Larsen, H. C., Johnsen, S., Masson-Delmotte, V., Stenni, B., Risi, C., Sodemann, H., et al. (2013). Continuous monitoring of summer surface water vapor isotopic composition above the Greenland ice sheet. *Atmospheric Chemistry and Physics*, 13(9), 4815–4828. <https://doi.org/10.5194/acp-13-4815-2013>
- Steen-Larsen, H. C., Masson-Delmotte, V., Hirabayashi, M., Winkler, R., Satow, K., Prié, F., et al. (2014). What controls the isotopic composition of Greenland surface snow? *Climate of the Past*, 10(1), 377–392. <https://doi.org/10.5194/cp-10-377-2014>
- Steen-Larsen, H. C., Sveinbjörnsdóttir, A., Jonsson, T., Ritter, F., Bonne, J.-L., Masson-Delmotte, V., et al. (2015). Moisture sources and synoptic to seasonal variability of north atlantic water vapor isotopic composition. *Journal of Geophysical Research: Atmospheres*, 120(12), 5757–5774. <https://doi.org/10.1002/2015jd023234>
- Town, M. S., Steen-Larsen, H. C., Wahl, S., Faber, A.-K., Behrens, M., Jones, T. R., & Sveinbjörnsdóttir, A. (2024). Post-depositional modification on seasonal-to-interannual timescales alters the deuterium-excess signals in summer snow layers in Greenland. *The Cryosphere*, 18(8), 3653–3683. <https://doi.org/10.5194/tc-18-3653-2024>
- Town, M. S., Walden, V. P., & Warren, S. G. (2007). Cloud cover over the south pole from visual observations, satellite retrievals, and surface-based infrared radiation measurements. *Journal of Climate*, 20(3), 544–559. <https://doi.org/10.1175/jcli4005.1>
- Town, M. S., Warren, S. G., Walden, V. P., & Waddington, E. D. (2008). Effect of atmospheric water vapor on modification of stable isotopes in near-surface snow on ice sheets. *Journal of Geophysical Research*, 113(D24). <https://doi.org/10.1029/2008jd009852>
- Vihma, T., Screen, J., Tjernström, M., Newton, B., Zhang, X., Popova, V., et al. (2016). The atmospheric role in the arctic water cycle: A review on processes, past and future changes, and their impacts. *Journal of Geophysical Research: Biogeosciences*, 121(3), 586–620. <https://doi.org/10.1002/2015jg003132>
- Wahl, S., Steen-Larsen, H. C., Hughes, A., Dietrich, L. J., Zühr, A., Behrens, M., et al. (2022). Atmosphere-snow exchange explains surface snow isotope variability. *Geophysical Research Letters*, 49(20), e2022GL099529. <https://doi.org/10.1029/2022gl099529>
- Wahl, S., Steen-Larsen, H. C., Reuder, J., & Hörhold, M. (2021). Quantifying the stable water isotopologue exchange between the snow surface and lower atmosphere by direct flux measurements. *Journal of Geophysical Research: Atmospheres*, 126(13), e2020JD034400. <https://doi.org/10.1029/2020jd034400>
- Worden, J., Noone, D., & Bowman, K. (2007). Importance of rain evaporation and continental convection in the tropical water cycle. *Nature*, 445(7127), 528–532. <https://doi.org/10.1038/nature05508>
- Worden, J. R., Kulawik, S. S., Fu, D., Payne, V. H., Lipton, A. E., Polonsky, I., et al. (2019). Characterization and evaluation of airs-based estimates of the deuterium content of water vapor. *Atmospheric Measurement Techniques*, 12(4), 2331–2339. <https://doi.org/10.5194/amt-12-2331-2019>
- Zolles, T., & Born, A. (2022). How does a change in climate variability impact the Greenland ice-sheet surface mass balance? *The Cryosphere Discussions*, 2022, 1–18.
- Zühr, A. M., Münch, T., Steen-Larsen, H. C., Hörhold, M., & Laepple, T. (2021). Local-scale deposition of surface snow on the Greenland ice sheet. *The Cryosphere*, 15(10), 4873–4900. <https://doi.org/10.5194/tc-15-4873-2021>
- Zühr, A. M., Wahl, S., Steen-Larsen, H. C., Hörhold, M., Meyer, H., & Laepple, T. (2023). A snapshot on the buildup of the stable water isotopic signal in the upper snowpack at eastgrip on the Greenland ice sheet. *Journal of Geophysical Research: Earth Surface*, 128(2), e2022JF006767. <https://doi.org/10.1029/2022jf006767>